1-1-1999

The effects of salts on polyelectrolyte systems.

Jonathan A. Zissu
University of Massachusetts Amherst

THE EFFECTS OF SALTS ON POLYELECTROLYTE SYSTEMS

A Dissertation Presented

by

JONATHAN A. ZISSU

Submitted to the Graduate School of the
University of Massachusetts Amherst in partial fulfillment
of the requirements for the degree of

DOCTOR OF PHILOSOPHY

September 1999

Department of Polymer Science and Engineering

THE EFFECTS OF SALTS ON POLYELECTROLYTE SYSTEMS

A Dissertation Presented

by

JONATHAN A. ZISSU

Approved as to style and content by:

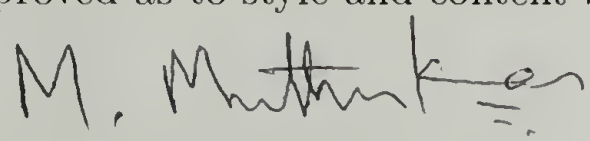

Murugappan Muthukumar, Chair

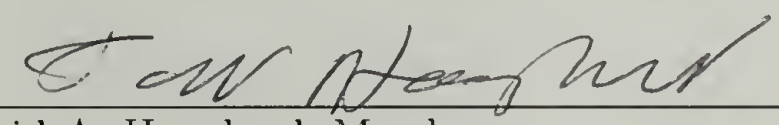

David A. Hoagland, Member

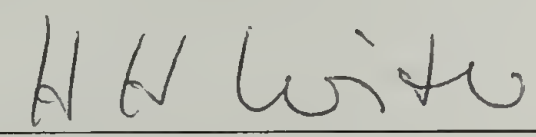

Henning H. Winter, Member

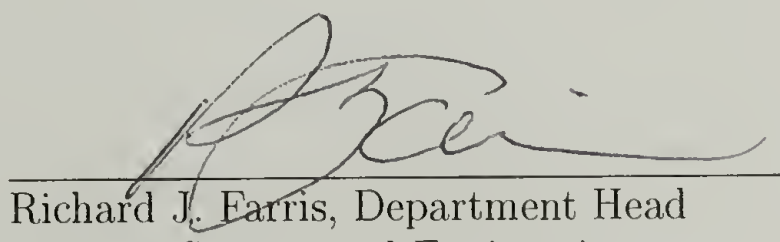

Richard J. Farris, Department Head
Polymer Science and Engineering

ACKNOWLEDGEMENTS

I would like to thank my dissertation committee members Prof. M. Muthukumar, Prof. D. Hoagland, and Prof. H. Winter for all of their help and for their patience with the process. I would especially like to thank my thesis advisor, Prof. M. Muthukumar, for all of his aid, both academic and personal, that he has given me over the years. I would also like to thank Friedeł von Goeler, Yvonne Akpalu, Joey Kong, Verna Lo, Paul Welch, Vivek Prabhu, and Radu Mondescu for being such wonderful associates, both in and out of the academic arena. I would finally like to thank Akzo-Nobel for sponsoring the work presented in these pages.

ABSTRACT

THE EFFECTS OF SALTS ON POLYELECTROLYTE SYSTEMS

SEPTEMBER 1999

JONATHAN A. ZISSU, M.S., UNIVERSITY OF MASSACHUSETTS

AMHERST

PH.D., UNIVERSITY OF MASSACHUSETTS AMHERST

Directed by: Professor M. Muthukumar

The effects of salts on the behavior of polyelectrolyte systems were investigated. The phase behavior of polyelectrolyte solutions in the presence of added salt was calculated by combining the free energies due to Flory-Huggins mixing and Debye-Hückel electrostatics, with both terms modified for our polyelectrolyte solutions. Using the calculated phase diagrams, we found that most results give a typical polymer-solvent-nonsolvent phase diagram, with the solvent acting as a "nonsolvent" (since we assume that the polymer-solvent interaction parameter, χ, is positive) and the dissociated salt acting as a "solvent". However, for high charges of the salt ions, we found a completely different phase diagram, one which can be explained by a "salting out effect" where the addition of salt over a certain concentration threshold causes complete phase separation over all concentrations of polymer and solvent. Also, the density and repulsive force profiles for a system comprised of two parallel, planar, uncharged surfaces uniformly covered with polyelectrolyte brushes in an electrolyte solution was calculated using a computational

enumeration of a one-dimensional random walk model. For large surface separations, we found three different density profiles: a Gaussian regime when κ is large, a stretched regime when κ is intermediate in value, and a "pancake" regime, with chains collapsed onto their grafted surface, when κ is small. For small surface separations, the first two regimes are replaced with an interpenetrating regime, where the density is essentially uniform across the entire region between the surfaces. For intermediate surface separations, the repulsive force scales as $\exp(-A\kappa^{\frac{1}{2}}D)$, unlike what is expected using Gouy-Chapman theory.

TABLE OF CONTENTS

LIST OF FIGURES

CHAPTER 1

INTRODUCTION

An area of growing importance in polymer science is the behavior of charged polymers, or polyelectrolytes. Whether dealing with polyacids and polybases, polyions and their copolymers, or polyampholytes, all of these are essentially polymers which can ionize in solution, thus creating a charged polymer chain. Of course, the charges on these chains will interact electrostatically with each other, as well as with the counterions derived from the ionization of the charged sites on the chains. This idea may be further extended to imply that introducing additional charged particles to our system, such as salts, will modify these interactions. Can these interactions be explicitly modelled and measured, and if so, how?

There are two basic methods for modelling these charged polymer systems. First, a particular polyelectrolyte chain in our system can be monitored to see what effect the charges along its backbone, as well as the rest of the system, has on its configuration. Since the configuration of the chain will affect the location of the charges along that chain, this method is a self-consistent field theory approach, which has been used by other researchers in this area [42, 45, 46]. This idea is the basis of the method used to model our polyelectrolyte brushes, consisting of two flat, parallel surfaces covered with grafted charged chains, all immersed in a salt solution. However, while a test chain is examined in great detail, the rest of the system, including solvent, salt, and even other polyelectrolyte chains, are all

grouped into a single mean-field background. In addition, while the configuration is sought for some systems, in others the phase behavior of the system may be more important, in which case the chain configuration is not at all useful.

Alternatively, instead of looking at a specific chain and its interactions with itself and its surrounding environment, the system can be monitored as a whole, accounting for all chemical species present in any relative amounts. This approach gives a much more general picture of what is happening, as all interactions between components will be described, not simply those between a polyelectrolyte chain and itself or the medium. This idea is the basis of the method used to model our polyelectrolyte solutions, with free polyelectrolyte chains immersed in a salt solution. Although this method is the more general, some approximations must be applied to make the theory manageable, including assuming that only pairwise and mean-field interactions are present and that the solution has a completely random distribution of each of the solution components. In fact, this may not be the case, especially if specific components tend to aggregate, such as in the case of counterion condensation. In addition, if any components are not free, such as in the case of grafted polyelectrolyte chains, this method will be insufficient to model that system, since all components are not equally distributed over the volume. Finally, only the behavior of the system as a whole will be derived by this method, so it is not possible to determine the configurations of the polymer chains or the local distributions of other solution components in our system using this technique.

This thesis dissertation focuses on two specific systems containing charged polymer and salt. Computational techniques, based upon theories specifically developed for these systems, are used to analyze various characteristics of those systems. Chapter 2 focuses on polyelectrolyte solutions, where all chemical species present, including the polymer chains, are allowed to explore the entire volume of the sys-

tem. The system is redefined in terms of a ternary solution and the phase behavior of the system is analyzed extensively. Chapter 3 focuses on polyelectrolyte brushes, where the polymer chains are grafted onto two flat, parallel surfaces, while the solvent, salt ions, and counterions to the polymer are considered free particles. This work is based upon the theory presented by F. von Goeler and M. Muthukumar for the system of a single surface covered with polyelectrolyte chains [51]. Both the density profiles for the brush and the force profile of the repulsion between these two covered surfaces are examined.

CHAPTER 2

POLYELECTROLYTE SOLUTIONS

2.1 Introduction

A polyelectrolyte will only ionize, thus becoming charged, if it is immersed in a solvent. In addition, it turns out that a very unusual effect is often seen in these charged polymer systems in the presence of added salt. Various experiments on polyelectrolyte solutions have been performed over the years, and it is known that if a salt-free polyelectrolyte solution is miscible, low concentrations of added salt will not greatly affect the miscibility. However, above a critical amount of salt, the whole solution spontaneously phase separates, and the polyelectrolyte precipitates out of solution. This property is commonly known as the "salting-out effect", and it is also known that salt ions of higher valence are more efficient at causing this effect. In an interesting article by Klooster, van der Touw, and Mandel [10], they describe an experiment where they measured the reduced viscosity of a poly(acrylic acid) solution as a function of the degree of neutralization, α', with sodium methoxide (CH_3ONa), a sodium salt of methanol. Up to a degree of neutralizaton of $\alpha' \leq 0.10$, the viscosity rises normally to a maximum value at $\alpha' = 0.10$. However, in the range $0.10 \leq \alpha' \leq 0.25$, they found that the viscosity drops sharply, much more than was expected. Furthermore, they found that the viscosity at $\alpha' \geq 0.25$ was actually lower than at initial conditions ($\alpha' = 0.00$). Although this phenomenon was not

specifically commented upon, it is reasonable to assume that this effect could be a result of the "salting-out effect", as described above.

Aside from experimental work, there has been some theoretical work on polyelectrolytes. Originally, all polymer solutions were assumed to behave according to Flory-Huggins theory [11]. This is a simple theory, assuming mean field liquid lattice interactions between the units of the polymer, the solvent molecules, and any other chemical species which are present in the solution, and in all pairwise combinations. For neutral systems, further modifications of this theory [12] have been proposed, especially in the pairwise interaction parameter, χ. However, this theory was only developed to model neutral polymers. Alternately, for solutions of electrolytes, Debye-Hückel theory can be applied to model the interactions between charges in solution. However, this theory only deals with small ions, and does not take into account the neutral units which may be present on the polyelectrolyte chains. Therefore, other theories have been proposed for polyelectrolyte solutions. For example, Skolnick and Fixman [14] derived a theory for a single polyelectrolyte chain in a salt solution. They assume a continuous charge distribution along a wormlike (stiff) polymer chain. In addition, they assume that they are working in the limit of low salt, and if this causes the chain to adopt a configuration in the rodlike limit, then excluded volume can be ignored. In addition, the charges interact via a screened Coulombic potential, as developed using the Debye-Hückel theory. By adding the electrostatic persistence length to the persistence length in the absence of electrostatic forces, they determined the total persistence length of the polyelectrolyte chain, which will dictate the average size of the polyelectrolyte. Soon after this theory was published, Odijk [15] developed his own theory of a polyelectrolyte chain in a salt solution. His derivation was similar to Skolnick and Fixman's theory, with a few improvements. He was able to generalize

his equations such that he could use any concentration of salt, which also removed the restriction to the rodlike limit. Therefore, he also incorporated the excluded volume of the chain in his theory. Finally, he allowed counterion condensation to occur. This means that if the chain has a continuous charge distribution along the chain, then the counterions (and the appropriately charged salt ions) would form a cylindrical "halo" around the chain. Again, the calculated electrostatic persistence length would modify the neutral persistence length to give the overall persistence length of the chain. More recently, Muthukumar [16] has developed a new theory of a polyelectrolyte chain in solution. Instead of looking at the potential, per unit charge, at the origin, as in Skolnick and Fixman's or Odijk's theories, he looks at the probability distribution function of a polyelectrolyte chain of a given contour length and end-to-end distance, which is given by the Edwards path integral. By using a variational procedure, the configuration of the polyelectrolyte chain can be determined in a self-consistent manner. Instead of explicitly determining the persistence length of the chain as a function of the solution conditions, he renormalizes the step length into a self-consistently defined function of the properties of the polyelectrolyte chain. This allows the use of almost any parameters in the Hamiltonian, such as salt concentration and excluded volume, and possibly even three-body interactions. Unfortunately, all three of these theories assumed that a polyelectrolyte solution can be modelled by a single chain in solution, ignoring any interchain interactions and concentrating on intrachain interactions only.

In this chapter, we investigate the phase diagrams of polyelectrolyte solutions in the presence of salt. To this end, we propose combining the Flory-Huggins theory of mixing, which will model the uncharged interactions in a ternary solution of polyelectrolyte (with counter-ions), salt (and their derivative ions), and solvent molecules, with Debye-Hückel theory of electrolytes in solution, which will model

the electrostatic interactions in the solution, to give the free energy of the solution. We can then minimize this free energy to find the coexistence curves at a given temperature with respect to polyelectrolyte chain length, Flory interaction parameter between polyelectrolyte and solvent, ionization of the polyelectrolyte, and the type of salt used.

2.2 Flory-Huggins Theory for Charged Polymers

Our system consists of a charged polymer in solution in the presence of salt, and is pictured in Figure 2.1. As we are dealing with a multicomponent polymer solution, the simplest starting point is the Flory-Huggins theory [11]. For our system, we will temporarily ignore all of the charges, and simply deal with the entropy and enthalpy of mixing of solvent molecules, polyelectrolyte molecules and their respective counterions, and each salt ion. We will also assume that all charged species will dissociate fully in solution. For our liquid lattice, we will define a liquid lattice site to be the size of our solvent molecule (eg. H_2O). Thus, our lattice is defined as consisting of n_0 sites, with each site having a size of $v_0 = v_1$, where v_1 is the molar volume of a solvent molecule. Finally, we note that all sites in our solution will be filled with some component of our solution; empty sites, or "holes" are not permitted in our theory. This will allow us to use number fractions identically with number fractions of the various components.

For our system, we have a minimum of five separate components in our solution: solvent, charged polymer, polymer counterions, and at least two salt ions after dissociation. While this can get very unruly to handle, we can remedy the problem by categorizing all units into one of three possible types: solvent (or component 1), polymer (component 2), or salt (component s). For the solvent, we have

n_1 molecules, and we have already defined each molecule to be of unit size for our lattice. For the polyelectrolyte, we have n_2 molecules, with each polymer chain identically made up of N segments, where we define a "segment" to be the size of a lattice site. In addition, when in solution, each polymer chain will have m charged sites, each of charge q, which in turn will give rise, from dissociation, to a single counterion of opposite charge $-q$ for each charged site, each of unit size. We will also define the degree of ionization of the polymer to be:

$$I = \frac{m}{N} \tag{2.1}$$

or the fraction of charged segments per polymer molecule. It should be noted that the original volume of the polymer, before dissociation, is therefore $N_2 = N+m$, not $N_2 = N$ as for neutral polymers. Finally, for the salt, we have n_s molecules, which will dissociate into γ different ions, with each ion of unit size. If for any specific ion γ there are n_γ ions of that type, then the original size of a salt molecule, or the total number of lattice sites that a salt molecule will occupy before dissociation, is given by:

$$N_s = \frac{\sum_\gamma n_\gamma}{n_s}. \tag{2.2}$$

We will also define the fraction of each ion γ of the salt to be:

$$r_{\gamma s} = n_\gamma / N_s n_s. \tag{2.3}$$

It shouls also be noted that because of the overall electroneutrality of the salt molecules:

$$\sum_\gamma n_\gamma Z_\gamma = 0 \tag{2.4}$$

where Z_γ is the valence of ion γ from the dissociated salt.

Now that we know the amount of each chemical species present, we can define the total volume, or total number of liquid lattice site, for our system to be simply

the sum of the size of each component multiplied by the number of molecules of that type, or:

$$n_0 = n_1 + Nn_2 + mn_2 + \sum_\gamma n_\gamma = n_1 + (1+I)Nn_2 + \sum_\gamma n_\gamma \tag{2.5}$$

where the first term represents the solvent, the second and third terms the polyelectrolyte (both the chain and counterions), and the fourth term the salt ions. When divided by the size of the system, n_0, this gives us a relationship between the mole fractions of the solvent ($\phi_1 = n_1/n_0$), polymer ($\phi_2 = Nn_2/n_0$), and salt ($\phi_s = N_s n_s = \sum_\gamma n_\gamma/n_0 = \sum_\gamma \phi_\gamma$):

$$\phi_1 + (1+I)\phi_2 + \phi_s = 1. \tag{2.6}$$

It is important to note that since we treat the counterions separately from the polyelectrolyte chain, we do not use the typical equation $\phi_1 + \phi_2 + \phi_3 = 1$ as in the case of neutral polymers. This will give a slight correction to any ternary phase diagrams we may calculate, but in regard to plotting the results, this will have little effect on the diagrams in the case of weakly charged polyelectrolytes ($I < 0.05$).

2.2.1 Entropy of Mixing

Now that we have defined our system, we can proceed to analyze the process of mixing. First, we will look at the entropy of our solution, which is defined by:

$$\begin{aligned} \Delta S_M &= k_B \ln\left[\frac{\Omega(n_1, n_2, INn_2, \sum_\gamma n_\gamma)}{\Omega(n_1,0,0,0)\Omega(0,n_2,0,0)\Omega(0,0,INn_2,0)\prod_\gamma \Omega(0,0,0,n_\gamma)}\right] \\ &= k_B \ln\left[\frac{\Omega}{\Omega_0}\right] = k_B[\ln\Omega - \ln\Omega_0] \end{aligned} \tag{2.7}$$

where Ω is the number of possible configurations of the mixed system, Ω_0 is the number of configurations of the unmixed system, keeping each chemical species separate from the others, and $\Omega(n_1, n_2, INn_2, \sum_\gamma n_\gamma)$ is the number of possible

configurations of placing n_1 solvent molecules, n_2 polymer molecules, INn_2 counterions, and $\sum_\gamma n_\gamma$ salt ions on a lattice of n_0 sites. Similarly, $\Omega(n_1, 0, 0, 0)$ is the number of configurations of n_1 solvent molecules on n_1 sites, $\Omega(0, n_2, 0, 0)$ is the number of configurations of n_2 polymer molecules on Nn_2 sites, $\Omega(0, 0, INn_2, 0)$ is the number of configurations of $INn_2 = mn_2$ counterions on INn_2 sites, and $\Omega(0, 0, 0, n_\gamma)$ is the number of configurations of n_γ salt ions of type γ on n_γ sites. It is easy to see that in the case of identical small ions filling a volume, there is only one way to place the molecules: one on each site until full. This means that $\Omega(n_1, 0, 0, 0) = \Omega(0, 0, INn_2, 0) = \Omega(0, 0, 0, n_\gamma) = 1$, which means that we can define $\Omega = \Omega(n_1, n_2, INn_2, \sum_\gamma n_\gamma)$ and $\Omega_0 = \Omega(0, n_2, 0, 0)$.

In order to calculate Ω, we must see how each separate component is added to our liquid lattice, beginning with the polymer chains. Let us define ν_i as the number of ways to place the i^{th} polymer chain onto our lattice of n_0 sites, assuming that $i - 1$ chains have already been placed. Furthermore, we will assume that the units of these chains are randomly distributed on our lattice, which is often referred to as the "mean field approximation". Thus, the total number of possible ways of placing n_2 identical chains on our lattice, which we will call Ω_2, is given by:

$$\Omega_2 = \frac{1}{n_2!} \prod_{i=1}^{n_2} \nu_i = \frac{1}{n_2!} \prod_{i=0}^{n_2-1} \nu_{i+1}. \tag{2.8}$$

Once the polymer chains have been placed on our lattice, the remaining available lattice sites can be filled, in turn, by solvent molecules, polymer counterions, and salt ions. By combinatorics, the total number of ways of placing these small molecules, each of unit size, on the $n_0 - Nn_2$ remaining sites, which we will call Ω_1, is given by:

$$\Omega_1 = \frac{(n_0 - Nn_2)!}{n_1!(INn_2)! \prod_\gamma (n_\gamma!)}. \tag{2.9}$$

Therefore, we can see that:

$$\Omega = \Omega_1 \Omega_2 = \frac{(n_0 - Nn_2)!}{n_1! n_2! (INn_2)! \prod_\gamma (n_\gamma!)} \prod_{i=0}^{n_2-1} \nu_{i+1}. \tag{2.10}$$

We must now calculate ν_{i+1} for our system. If there are i chains that have already been placed, then we know that Ni sites are occupied, and the fraction of filled sites, which we label as f_i, is given by:

$$f_i = \frac{Ni}{n_0} \tag{2.11}$$

and from the mean field approximation, we will assume that these sites are randomly distributed throughout the system. When we place the first segment of the $(i+1)^{\text{st}}$ chain into this system, there are $n_0 - Ni$ available sites. If we assume that each site in our liquid lattice hase z nearest-neighbors, then the second segment of the chain must occupy one of the adjoining sites to that of the first segment. However, we must also take into account that some of the sites are already filled by segments of previously placed chains, so the second segment will have a choice of $z(1 - f_i)$ possible sites, where $(1 - f_i)$ is the fraction of unfilled sites in our system after i chains have already been placed. Similarly, the third segment must be placed in an unoccupied nearest-neighbor to the second segment, with the exception of the site occupied by the first segment. This gives a choice of $(z - 1)(1 - f_i)$ sites for the third segment. Each succeeding segment will have a similar choice to the third, or $(z - 1)(1 - f_i)$ possible sites. Since each chain is made up of N segments, the number of ways of placing the $(i + 1)^{\text{st}}$ is then the product of each of these steps, or:

$$\nu_{i+1} = (n_0 - Ni) z (z - 1)^{N-2} (1 - f_i)^{N-1}. \tag{2.12}$$

Since we are using a liquid lattice, we can assume that each site has a large number

of nearest-neighbors, or $z \approx z - 1$, and substituting (2.11) we find:

$$\nu_{i+1} = (n_0 - Ni)^N \left(\frac{z-1}{n_0}\right)^{N-1} \tag{2.13}$$

which may then be substituted into (2.10).

We can see that in order to calculate the entropy of mixing, we need to take the logarithm of Ω. First, we can see that:

$$\ln \prod_{i=0}^{n_2-1} \nu_{i+1} = (N-1)n_2 \ln\left(\frac{z-1}{n_0}\right) + N \sum_{i=0}^{n_2-1} \ln(n_0 - Ni) \tag{2.14}$$

where the first term arises from the i-independent prefactor of ν_{i+1}. If we have a sufficiently large number of chains in our solution, we can approximate the sum in our second term by an integral:

$$\begin{aligned} \ln \prod_{i=0}^{n_2-1} \nu_{i+1} &= (N-1)n_2 \ln\left(\frac{z-1}{n_0}\right) + N \int_0^{n_2} di \ln(n_0 - Ni) \\ &= (N-1)n_2 \ln\left(\frac{z-1}{n_0}\right) + n_0 \ln n_0 - n_0 - \\ &\quad (n_0 - Nn_2)\ln(n_0 - Nn_2) + (n_0 - Nn_2). \end{aligned} \tag{2.15}$$

Next, for the logarithm of the prefactor to $\prod \nu_i$, we will use Sterling's approximation, which states:

$$\ln X! \approx X \ln X - X \tag{2.16}$$

for sufficiently large values of X. By using (2.15) and (2.16), and taking the logarithm of (2.10), we find:

$$\begin{aligned} \ln \Omega &= n_0 \ln n_0 - n_0 - n_1 \ln n_1 + n_1 - n_2 \ln n_2 + n_2 - INn_2 \ln(INn_2) + \\ &\quad INn_2 - \sum_\gamma n_\gamma \ln n_\gamma + \sum_\gamma n_\gamma + (N-1)n_2 \ln\left(\frac{z-1}{n_0}\right). \end{aligned} \tag{2.17}$$

It should be noted that the $n_0 - Nn_2$ terms arising from ν_{i+1} and $(n_0 - Nn_2)!$ cancel each other out. Similarly, for the Ω_0 term in (2.7), we can use the same technique as in Ω, except that only the polymer chains are present. For this case, we will

assume that $n_1 = n_\gamma = 0$, that there are no counterions to the polymer, and that the total size of the system is therefore $n_0 = Nn_2$. Substituting these values into (2.10), we find a similar expression for Ω_0:

$$\Omega_0 = \frac{1}{n_2!} \prod_{i=0}^{n_2-1} \nu'_{i+1} \tag{2.18}$$

where:

$$\nu'_{i+1} = (Nn_2 - Ni)^N \left(\frac{z-1}{Nn_2}\right)^{N-1}. \tag{2.19}$$

Following the procedure outlined above, taking the logarithm of (2.18) yields:

$$\ln \Omega_0 = Nn_2 \ln(Nn_2) - Nn_2 - n_2 \ln n_2 + n_2 + (N-1)n_2 \ln\left(\frac{z-1}{Nn_2}\right). \tag{2.20}$$

We can now substitute (2.17) and (2.20) into (2.7). If we expand n_0 by applying (2.5), expand all logarithms, cancel out appropriate terms, and regroup appropriate logarithms, we find an initial expression for the entropy of mixing:

$$\frac{\Delta S_M}{k_B} = -n_1 \ln \phi_1 - n_2 \ln \phi_2 - INn_2 \ln(I\phi_2) - \sum_\gamma n_\gamma \ln \phi_\gamma. \tag{2.21}$$

We will finally rewrite this equation solely in terms of the mole fractions of our three basic components, by using $r_{\gamma s}$ and n_0 and noting that $\sum_\gamma r_{\gamma s} = 1$, to find our final expression for the entropy of mixing:

$$\begin{aligned} \frac{\Delta S_M}{k_B} &= -n_0 \left[\phi_1 \ln \phi_1 + \frac{\phi_2}{N} \ln \phi_2 + I\phi_2 \ln(I\phi_2) + \right. \\ &\qquad \left. \phi_s(\ln \phi_s + \sum_\gamma r_{\gamma s} \ln r_{\gamma s})\right]. \end{aligned} \tag{2.22}$$

2.2.2 Enthalpy and Free Energy of Mixing

We now turn our attention to the enthalpy of mixing for our system. First, we will assume that only the non-ionic interactions will be important. This allows us to ignore all interactions involving the counterions and salt ions for this calculation,

and only the polymer segments and solvent molecules will be considered. Charge interactions (both charge-charge and dielectric) will be dealt with separately. Also, we will again assume that mean field theory applies for this calculation, as in the entropy calculation. Finally, we will assume that only nearest-neighbor interactions are important for the enthalpy of mixing, where we will again use the same liquid lattice as described above.

As we are only considering non-ionic interactions of polymer and solvent molecules, there are only three possible interaction pairs: solvent-solvent, polymer-polymer, and solvent-polymer. Let us define ω_{11} as the energy of interaction between two nearest-neighbor solvent molecules, ω_{22} as the energy of interaction between two unconnected nearest-neighbor polymer segments, and ω_{12} as the energy of interaction between a solvent molecule and a polymer segment which are nearest-neighbors. We will first look at the unmixed system (i.e. pure solvent and pure polymer). Since there are n_1 solvent molecules on n_1 sites before mixing, there will be $\frac{1}{2}zn_1$ solvent-solvent interactions, where z is again the number of nearest-neighbors in our liquid lattice, and the factor of $\frac{1}{2}$ is used to avoid double-counting interactions between identical molecules. Similarly, since there are Nn_2 polymer segments on Nn_2 sites before mixing, there will be $\frac{1}{2}(z-2)Nn_2$ polymer-polymer interactions, where we now use $(z-2)$ instead of z because of the connectivity of the polymer, ignoring any chain ends.

Now we will look at our mixed system. It should be noted that although we are only considering solvent and polymer molecules, the size of our mixed system is still n_0. If we look at a site with a polymer segment, then on average, there will be $(z-2)\phi_1$ nearest-neighbor solvent molecules, where ϕ_1 is the fraction of sites (out of n_0 total sites) filled with a solvent molecule in the mixed state, and the $(z-2)$ prefactor takes into account the connectivity of the polymer, as in the unmixed state.

Since there is a total of Nn_2 polymer segments in our solution, the average number of polymer-solvent interactions will be given by $(z-2)\phi_1 Nn_2$. Similarly, there will be $\frac{1}{2}z\phi_1 n_1$ solvent-solvent interactions and $\frac{1}{2}(z-2)\phi_2 Nn_2$ polymer-polymer interactions, on average. Again, the factor of $\frac{1}{2}$ is used to avoid double-counting interactions between two identical units.

If we again assume that z is sufficiently large, as in the entropy calculations, then we can replace $(z-2)$ by z. This assumption has the added benefit of taking the chain ends of the polymer into account in any further calculations. The enthalpy of mixing is then given by the change in energy between the mixed and unmixed states, or:

$$\begin{aligned}
\Delta H_M &= (z\phi_1 Nn_2\omega_{12} + \frac{1}{2}z\phi_1 n_1\omega_{11} + \frac{1}{2}z\phi_2 Nn_2\omega_{22}) - \\
&\quad (\frac{1}{2}zn_1\omega_{11} + \frac{1}{2}zNn_2\omega_{22}) \\
&= z\phi_1 Nn_2\omega_{12} + \frac{1}{2}z\phi_1\omega_{11}\left(n_1 - \frac{n_1}{\phi_1}\right) + \frac{1}{2}z\phi_2\omega_{22}\left(Nn_2 - \frac{Nn_2}{\phi_2}\right) \\
&= z\phi_1 Nn_2\omega_{12} + \frac{1}{2}z\phi_1\omega_{11}(Nn_2 + INn_2 + \sum_\gamma n_\gamma) + \\
&\quad \frac{1}{2}z\phi_2\omega_{22}(n_1 + INn_2 + \sum_\gamma n_\gamma). \qquad (2.23)
\end{aligned}$$

Since we have already stated that we will ignore all counterions and salt ions, we will assume that we can ignore all terms beyond the first in both sets of parentheses in the last equation. This then gives us:

$$\begin{aligned}
\Delta H_M &= z\phi_1 Nn_2\omega_{12} - \frac{1}{2}z\phi_1 Nn_2\omega_{11} - \frac{1}{2}z\phi_2 n_1\omega_{22} \\
&= zn_0\phi_1\phi_2\omega_{12} - \frac{1}{2}zn_0\phi_1\phi_2\omega_{11} - \frac{1}{2}zn_0\phi_1\phi_2\omega_{22}. \qquad (2.24)
\end{aligned}$$

If we define $\Delta\omega$ to be the energy lost in making a pair of polymer-solvent interactions from a solvent-solvent interaction and a polymer-polymer interaction, or:

$$\Delta\omega = \omega_{11} + \omega_{22} - 2\omega_{12} \qquad (2.25)$$

and defining the Flory interaction parameter (χ) as:

$$\chi = -\frac{z\Delta\omega}{2k_BT} \tag{2.26}$$

we can rewrite (2.24) to give us our final expression for the enthalpy of mixing:

$$\frac{\Delta H_M}{k_BT} = \chi n_0 \phi_1 \phi_2. \tag{2.27}$$

The free energy of mixing is defined in terms of the entropy and enthalpy of mixing to be:

$$\Delta G_M = \Delta H_M - T\Delta S_M. \tag{2.28}$$

Instead of using this expression, it is more useful to calculate a dimensionless free energy per site:

$$\left.\frac{\Delta G_M}{k_BT}\right|_{site} = \frac{1}{n_0}\left(\frac{\Delta G_M}{k_BT}\right) = \frac{1}{n_0}\left(\frac{\Delta H_M}{k_BT} - \frac{\Delta S_M}{k_B}\right). \tag{2.29}$$

Upon substituting (2.22) and (2.27) into (2.29), we arrive at our final expression for the free energy of mixing for our system:

$$\begin{aligned}\left.\frac{\Delta G_M}{k_BT}\right|_{\text{site}} &= \phi_1 \ln \phi_1 + \frac{\phi_2}{N}\ln\phi_2 + I\phi_2 \ln(I\phi_2) + \\ &\quad \phi_s(\ln\phi_s + \sum_\gamma r_{\gamma s}\ln r_{\gamma s}) + \chi\phi_1\phi_2.\end{aligned} \tag{2.30}$$

2.3 Debye-Hückel Theory for Charged Polymers

So far, we have dealt with the free energy of mixing while ignoring the effects of the charges in the system. We will now turn our attention to the electrolytic properties of a polyelectrolyte solution in the presence of salt. To this end, we will use a modified version of the Debye-Hückel theory for a solution of small-molecule electrolytes [13], as this is probably the simplest theory for a solution of charges.

We will also use the variables as defined above, as well as (2.1)-(2.6) from that section. Finally, we will assume the polymer chain to be a single large unit of total size N and total charge mq, to make our conversions from number densities to volume fractions of each component a bit easier.

2.3.1 Pair Distribution Function and Debye Screening Length

Let us consider a solution of charged particles, which we will label as α, β, and so forth. It should be noted that there will be at least two ions, as any salt molecule must dissociate, in solution, into at least one negatively charged ion for each positively charged ion, and vice versa. In addition, the overall electroneutrality of the solution must hold not only for the salt molecules, but for all charged species, including charges arising from the polyelectrolyte. In terms of the number densities of these ions, this gives us:

$$\sum_{\gamma} eZ_{\gamma}\rho_{\gamma} = 0 \tag{2.31}$$

where rg is the number density of ion γ in solution, Z_{γ} is the valence of that ion, and e is the charge of a single electron. In this equation, γ may represent a salt ion, a charged polymer molecule, or a counterion to the charged polymer. Finally, it should also be noted that the relation between the number density and volume fraction of a particular component is:

$$\phi_{\gamma} = \mathrm{v}_1 N_{\gamma}\rho_{\gamma} \tag{2.32}$$

where ϕ_{γ} is the volume fraction of a particular component, v_1 is both the molar volume of a solvent molecule and the size of a volume element, as defined above for the Flory-Huggins theory, and N_{γ} is the size of the specified component.

Let us pretend that we are working with only two charges suspended in a vacuum. Therefore, there is nothing that will diminish the Coulombic interaction

between the two ions. If we specify ion α to be at the origin of our coordinate system, then ion β must be at some position $\vec{r}$ away from the origin. The probability that the ions are at a distance of $r = |\vec{r}|$ from each other, which we will call $\gamma_{\beta\alpha}$, is then given by Boltzmann statistics:

$$\gamma_{\beta\alpha}(r) = \exp\left(-\beta\frac{e^2 Z_\alpha Z_\beta}{r}\right) \tag{2.33}$$

where $\beta = \frac{1}{k_B T}$ when not used as a subscript. It is easy to see that while this has been developed for ion α at the origin and ion β at $\vec{r}$, the same equation may also be applied to ion β at the origin and ion α at $\vec{r}$, by symmetry. We can generalize this equation for any number of charges in any medium:

$$\gamma_{\beta\alpha}(r) = \exp[-\beta e Z_\beta \Phi_\alpha(r)] \tag{2.34}$$

where $\Phi_\alpha(r)$ represents the electric potential at $\vec{r}$ due to the ion of type α at the origin, all the other ions in the solution, and the effect of the medium through its dielectric constant, ε. It is important to note that since the direction of displacement of ion β is unimportant, $\Phi_\alpha(r)$ will depend only upon its distance from the origin, not the direction. This is especially true in the case of mean field theory, which we will again assume to hold for our system. While the probability distribution function is a useful quantity, a more useful quantity to calculate is the pair distribution function, $n_{\alpha\beta}$, which is defined as:

$$n_{\alpha\beta} = \rho_\alpha \rho_\beta \gamma_{\beta\alpha} \tag{2.35}$$

and is again only dependent upon the distance between ion α, at the origin, and ion β, away from the origin.

First, we must find the expression for electric field in our system, $\Phi_\alpha(r)$, due to an ion α at the origin and all other ions throughout the system. For this theory, we

will assume that Poisson electrostatics is valid on all length scales, including the microscopic. While this assumption is arguable, our mean field theory assumption makes this choice fairly straightforward. This assumption allows us to define the electric field in terms of the charge density:

$$\nabla^2 \Phi_\alpha(r) = -\frac{4\pi}{\varepsilon} q_\alpha(r) \tag{2.36}$$

where $q_\alpha(r)$ is the charge density at a distance of r from the origin, and is defined by:

$$q_\alpha(r) = eZ_\alpha \delta(r) + \sum_\gamma eZ_\gamma \rho_\gamma \gamma_{\gamma\alpha}(r) \tag{2.37}$$

where $\delta(r)$ is the Dirac delta function about the origin. The first term of this equation represents the charge density due to the ion α at the origin, while the second term represents all other ions in our system, away from the origin at a distance of r. Substituting (2.34) and (2.37) into (2.36), we find:

$$\nabla^2 \Phi_\alpha(r) = -\frac{4\pi e}{\varepsilon} Z_\alpha \delta(r) - \frac{4\pi e}{\varepsilon} \sum_\gamma Z_\gamma \rho_\gamma \exp[-\beta e Z_\gamma \Phi_\alpha(r)]. \tag{2.38}$$

There is a slight problem with this definition, however. At the start, we arbitrarily defined ion α to be at the origin, with all other ions elsewhere. However, this coordinate system should not affect the electric field at any point, no matter what ion we defined to exist at the origin. Therefore, we would like to remove our dependence of the electric field on the type of ion at the origin, and therefore on the valence of that ion. In order to make our equations agree with this, we note that at equilibrium, the probability distribution function should not depend upon which of the two interacting ions is at the origin; only the distance between those ions will determine the probability distribution. In other words:

$$\gamma_{\beta\alpha}(r) = \gamma_{\alpha\beta}(r) \tag{2.39}$$

$$Z_\beta \Phi_\alpha(r) = Z_\alpha \Phi_\beta(r). \tag{2.40}$$

We will therefore define our electric field, by using (2.40), as:

$$\Phi(r) = \frac{1}{Z_\alpha}\Phi_\alpha(r) \tag{2.41}$$

where $\Phi(r)$ is independent of the type of ion at the origin. Rewriting (2.38) in terms of our coordinate-independent electric field, we find:

$$\nabla^2\Phi(r) = -\frac{4\pi e}{\varepsilon}\delta(r) - \frac{4\pi e}{\varepsilon Z_\alpha}\sum_\gamma Z_\gamma\rho_\gamma \exp[-\beta e Z_\gamma \Phi(r)]. \tag{2.42}$$

Unfortunately, since $\Phi(r)$ is defined self-consistently above, we can see that our expression is *not* independent of Z_α, thus contradicting our assumption.

Obviously, something more must be done to make our electric fields independent of the ion at the origin. In order to do this, we must assume that the electric fields in our system are weak, which corresponds to a dilute electroyte solution. If this is true, then we can expand the exponential term in (2.42) with a Taylor series about a point $\Phi(r) = 0$:

$$\begin{aligned}
\nabla^2\Phi(r) &= -\frac{4\pi e}{\varepsilon}\delta(r) - \frac{4\pi e}{\varepsilon Z_\alpha}\sum_\gamma Z_\gamma\rho_\gamma[1 - \beta e Z_\gamma\Phi(r)] \\
&= -\frac{4\pi e}{\varepsilon}\delta(r) - \frac{4\pi e}{\varepsilon Z_\alpha}\sum_\gamma Z_\gamma\rho_\gamma + \\
&\quad \left(\frac{4\pi e^2\beta}{\varepsilon}\sum_\gamma Z_\gamma^2\rho_\gamma\right)\Phi(r)
\end{aligned} \tag{2.43}$$

and by using (2.31), we can eliminate the second term, giving:

$$\nabla^2\Phi(r) = -\frac{4\pi e}{\varepsilon}\delta(r) + \kappa^2\Phi(r) \tag{2.44}$$

where κ is called the Debye screening length, and is defined as:

$$\kappa^2 = \frac{4\pi e^2\beta}{\varepsilon}\sum_\gamma Z_\gamma^2\rho_\gamma. \tag{2.45}$$

It is easy to see that (2.44) is now explicitly independent of Z_α, agreeing with our previous assumption.

In order to solve this equation, we first note that as we move away from a charge, the electric field arising from that charge drops off sharply. Similarly, as we move away from our solution, the overall electric field arising from the charges will be minimal, or:

$$\Phi(r) \to 0 \text{ as } r \to \infty \tag{2.46}$$

which in turn allows us to use Fourier transformations to solve our equations. Transforming our equation and regrouping terms, we find:

$$\Phi_k = \frac{4\pi e}{\varepsilon} \frac{1}{k^2 + \kappa^2} \tag{2.47}$$

where $\vec{k}$ is the wave vector which is conjugate to $\vec{r}$, and $k = |\vec{k}|$. We now use this expression in our reverse Fourier transformation, using spherical coordinates:

$$\Phi(r) = \frac{4\pi e}{8\pi^3 \varepsilon} \int_0^{2\pi} d\phi \int_{-1}^{1} dx \int_0^{\infty} \frac{k^2 dk \exp(-ikrx)}{k^2 + \kappa^2} \tag{2.48}$$

where ϕ represents the polar angle, $x = \cos\theta$, where θ represents the azimuthal angle, and $i = \sqrt{-1}$. Since (2.47) depends only on k, and using complex contour integration, we eventually find:

$$\Phi(r) = \frac{e}{\varepsilon r} \exp(-\kappa r). \tag{2.49}$$

Finally, substituting (2.49), (2.41), and (2.34) into (2.35), we find our final expression for $n_{\alpha\beta}$:

$$n_{\alpha\beta}(r) = \rho_\alpha \rho_\beta \left[1 - \frac{\beta e^2 Z_\alpha Z_\beta}{\varepsilon r} \exp(-\kappa r)\right] \tag{2.50}$$

where we have expanded $\gamma_{\beta\alpha}$ in a Taylor series about $\Phi(r) = 0$, as we did for (2.43). Again, since we assume a dilute electrolyte solution, this expansion is permitted.

2.3.2 Excess Electrostatic Free Energy

Now that we know $n_{\alpha\beta}$, we can calculate the free energy of our system arising from the charges. Let us define M as the total number of particles in our system:

$$M = \sum_{\gamma} M_{\gamma} + M_0 \tag{2.51}$$

where $M_0 = n_1$ is the number of solvent molecules and $\sum_{\gamma} M_{\gamma}$ is the total number of charged particles in our system, including the salt ions, polyeletrolyte molecules *as a whole*, and counterions to the polymer. We will define our partition function, Z_M, as:

$$Z_M = \left(\frac{2\pi p}{\beta h^2}\right)^{\frac{3M}{2}} Q_M \tag{2.52}$$

where p is the average mass of a particle, h is Planck's constant, and Q_M is the configurational integral for our system:

$$Q_M = \frac{1}{\prod_{\gamma} M_{\gamma}! M_0!} \int d\vec{r_1} \cdots d\vec{r_M} \exp(-\beta U_M) \exp(-\beta \lambda V_M). \tag{2.53}$$

Here, U_M represents all non-Coulombic long-ranged interactions in our system, $V_M = \sum_{i>j} \frac{e^2 Z_i Z_j}{r_{ij}}$ represents the Coulombic interactions between all possible pairs of charged particles, and λ represents the strength of the Coulombic interactions, where $\lambda = 1$ refers to all charges interacting normally and $\lambda = 0$ refers to all charges "turned off" in the system. We will denote $\lambda = 0$ as our "reference system", and the particles will interact without their usual charges.

We can write the electrolytic free energy per unit volume in terms of our partition function:

$$\frac{F_E}{n_0 \mathrm{v}_1} = -\frac{1}{\beta n_0 \mathrm{v}_1} \ln Z_M \tag{2.54}$$

where $n_0 \mathrm{v}_1$ is the total volume of the system as defined for the Flory-Huggins calculations. As in the case of our Flory-Huggins calculations, however, we do not

want the electrostatic free energy, but the excess electrostatic free energy relative to our reference system, with all charges turned off:

$$\begin{aligned}\frac{\Delta F_E}{n_0 \mathrm{v}_1} &= \frac{F_E}{n_0 \mathrm{v}_1} - \frac{F_E^0}{n_0 \mathrm{v}_1} \\ &= -\frac{1}{\beta n_0 \mathrm{v}_1}[\ln Q_M(\lambda = 1) - \ln Q_M(\lambda = 0)] \end{aligned} \tag{2.55}$$

where the prefactor of (2.52) drops out conveniently. If we define $F_E(\lambda) = -\frac{1}{\beta} \ln Q_M(\lambda)$, it is easy to see from (2.53) that:

$$\begin{aligned}\frac{1}{n_0 \mathrm{v}_1} \frac{\partial F_E(\lambda)}{\partial \lambda} &= \frac{1}{n_0 \mathrm{v}_1} \frac{\int d\vec{r_1} \cdots d\vec{r_M} V_M \exp(-\beta U_M) \exp(-\beta \lambda V_M)}{\int d\vec{r_1} \cdots d\vec{r_M} \exp(-\beta U_M) \exp(-\beta \lambda V_M)} \\ &= \frac{1}{n_0 \mathrm{v}_1} \frac{\langle \lambda V_M \rangle_\lambda}{\lambda} \end{aligned} \tag{2.56}$$

where $\langle \cdots \rangle_\lambda$ is the average over probability distribution:

$$P_M(\lambda) = \frac{\exp(-\beta U_M) \exp(-\beta \lambda V_M)}{\int d\vec{r_1} \cdots d\vec{r_M} \exp(-\beta U_M) \exp(-\beta \lambda V_M)}. \tag{2.57}$$

We can now rewrite (2.55) in terms of an integral over λ, using (2.56), to get:

$$\frac{\Delta F_E}{n_0 \mathrm{v}_1} = \frac{1}{n_0 \mathrm{v}_1} \int_0^1 \frac{d\lambda}{\lambda} \langle \lambda V_M \rangle_\lambda = \frac{1}{2} \int_0^1 \frac{d\lambda}{\lambda} \int d\vec{r} \sum_{\alpha,\beta} \lambda V_{\alpha\beta}(r) n_{\alpha\beta}(r; \lambda) \tag{2.58}$$

where the sum is over all charge pairs in the system, with the factor of $\frac{1}{2}$ to avoid double-counting, and $n_{\alpha\beta}(r; \lambda)$ is the pair distribution function derived from (2.57), not (2.50).

At this point, we need to make two important assumptions. First, we note that since U_M is mainly seen through the dielectric constant of the solvent, we can instead rewrite our pair Coulombic interaction term, $V_{\alpha\beta}$, as:

$$\frac{e^2 Z_\alpha Z_\beta}{r_{\alpha\beta}} \rightarrow \frac{e^2 Z_\alpha Z_\beta}{\varepsilon r_{\alpha\beta}} \tag{2.59}$$

and take $U_M = 0$. While there is no direct proof why this assumption should be valid, it is necessary to make this assumption for our calculations. Second, we

would like to use $n_{\alpha\beta}$ as derived in (2.50) instead of from (2.57). If we define:

$$\frac{\Delta\tilde{F}_E}{n_0 \mathrm{v}_1} = \frac{1}{2}\int_0^1 \frac{d\lambda}{\lambda}\int d\vec{r}\sum_{\alpha,\beta}\lambda V_{\alpha\beta}(r)\tilde{n}_{\alpha\beta}(r;\lambda) \tag{2.60}$$

where $V_{\alpha\beta}$ is our new screened potential, defined by (2.59), and $\tilde{n}_{\alpha\beta}(r;\lambda)$ is the pair distribution function for the screened potential $V_{\alpha\beta}$ with $U_M = 0$. We will now assume:

$$\Delta F_E \rightarrow \Delta\tilde{F}_E \tag{2.61}$$

$$\{\rho_\alpha\} \rightarrow 0 \tag{2.62}$$

which is asymptotically valid in the limit of highly dilute solutions. Upon comparison of $\tilde{n}_{\alpha\beta}(r;\lambda)$ with the desired $n_{\alpha\beta}(r)$ from (2.50), we find:

$$\tilde{n}_{\alpha\beta}(r;\lambda = 1) = n_{\alpha\beta}(r) \tag{2.63}$$

and for the charges not fully "turned on", or $0 \leq \lambda < 1$, we can use a formal transformation of (2.50):

$$e^2 \rightarrow \lambda e^2. \tag{2.64}$$

Now we can substitute (2.64) and (2.50) into (2.60) to get:

$$\begin{aligned}\frac{\Delta\tilde{F}_E}{n_0 \mathrm{v}_1} &= \frac{1}{2}\int_0^1 \frac{d\lambda}{\lambda}\int d\vec{r}\sum_{\alpha,\beta}\frac{\lambda e^2 Z_\alpha Z_\beta}{\varepsilon r}\rho_\alpha\rho_\beta \times \\ &\quad \left[1 - \frac{\beta\lambda e^2 Z_\alpha Z_\beta}{\varepsilon r}\exp(-\lambda^{\frac{1}{2}}\kappa r)\right]\end{aligned} \tag{2.65}$$

and using (2.31), this integral simplifies to give us an expression for the excess electrostatic free energy for our system:

$$\frac{\Delta F_E}{n_0 \mathrm{v}_1} = \frac{\Delta\tilde{F}_E}{n_0 \mathrm{v}_1} = -\frac{\kappa^3 k_B T}{12\pi} \tag{2.66}$$

where as an analogy to (2.30), $\frac{\Delta F_E}{n_0 \mathrm{v}_1} = \frac{\Delta G_E}{n_0 \mathrm{v}_1} = \Delta G_E|_{\mathrm{site}}$.

2.4 Polyelectrolyte Solutions and Phase Diagrams

Because the mixing free energy and electrostatic free energy, as we have derived above for our system, were developed to be independent of one another, we assume that we can simply add the two energies together to get the overall free energy of our system:

$$\left.\frac{\Delta G}{k_B T}\right|_{\text{site}} = \left.\frac{\Delta G_M}{k_B T}\right|_{\text{site}} + \left.\frac{\Delta G_E}{k_B T}\right|_{\text{site}} \tag{2.67}$$

with our reference state taken to be unmixed and electrically neutral. If we substitute (2.30) and (2.66) into (2.67), we arrive at our final expression for the free energy of our polyelectrolyte solution:

$$\begin{aligned}\left.\frac{\Delta G}{k_B T}\right|_{\text{site}} &= \phi_1 \ln \phi_1 + \frac{\phi_2}{N} \ln \phi_2 + I\phi_2 \ln(I\phi_2) + \\ &\quad \phi_s(\ln \phi_s + \sum_\gamma r_{\gamma s} \ln r_{\gamma s}) + \chi\phi_1\phi_2 - \frac{\kappa^3}{12\pi}\end{aligned} \tag{2.68}$$

where κ may be defined in terms of the volume fractions of the three basic components of our system by substituting (2.32) into (2.45):

$$\kappa^2 = \frac{4\pi e^2 \beta}{\varepsilon \mathrm{v_I}}[(\sum_\gamma Z_\gamma^2 r_{\gamma s})\phi_s + Iq^2(m+1)\phi_2]. \tag{2.69}$$

For the equation for κ, the first term represents the contribution of the salt ions, while the second term represents the contribution of both the charged polymer, of total size N and total charge mq, and the counterions to the polymer, each of size 1 and charge q.

Now that we have an expression for the free energy of our solution, we can calculate our phase diagrams, given particular values for N, m, χ, $\frac{4\pi e^2\beta}{\varepsilon \mathrm{v_1}}$, and values of Z_γ and $r_{\gamma s}$ for each salt ion. The normal way to do this is to calculate the chemical potential, μ, for each separate chemical species, with respect to its reference state:

$$\begin{aligned} \mu_1 - \mu_1^0 &= \frac{\partial \Delta G}{\partial n_1} \\ \mu_2 - \mu_2^0 &= \frac{\partial \Delta G}{\partial n_2} \\ \mu_s - \mu_s^0 &= \frac{\partial \Delta G}{\partial n_s} \end{aligned} \tag{2.70}$$

and for two separate compositions in phase equilibrium, we will solve the following set of equations:

$$\begin{aligned} \mu_1 &= \mu_1' \\ \mu_2 &= \mu_2' \\ \mu_s &= \mu_s'. \end{aligned} \tag{2.71}$$

Unfortunately, when we tried to use this method to calculate our phase diagrams, the only points that we were able to find that satisfied these equations were homogeneous points, or $\phi_1 = \phi_1'$, $\phi_2 = \phi_2'$, and $\phi_s = \phi_s'$. While these points are obviously viable solutions to our equation, they do not give us any useful data with which we can find a phase-separated region of our phase diagram.

Another method is needed, therefore, to find the two-phase region (or regions) of our diagram. In order to solve this problem, we use the reverse of our original idea; instead of trying to find a stable tie line in a two-phase region by using our equations, we will instead begin with a random tie line and use our equations to make it stable. An example of an initial tie line is given in Figure 2.2. Each tie line is based on a legal composition, represented by a point which we will call C. The tie line is then drawn through this point, extending a length of a away from C to one side, ending at a point we will call B, and a length of b to the other side, ending at a point we will call A. Finally, the tie line makes some angle with the horizontal (solvent) axis, which we will call θ_1. It should be noted that the other two angles are closely related to θ_1; if we want to find the angle the tie line makes

with the polymer axis, we find $\theta_2 = \theta_1 + \frac{\pi}{3}$. Using a, b, and θ_1, we can calculate the compositions at points A and B, given the composition at C:

$$A_1 = C_1 + b\sin\theta_1 \tag{2.72}$$

$$A_2 = C_2 - b\sin\theta_2 \tag{2.73}$$

$$B_1 = C_1 - a\sin\theta_1 \tag{2.74}$$

$$B_2 = C_2 + a\sin\theta_2 \tag{2.75}$$

where $A_1 = \phi_{1,A}$ represents the mole fraction of component 1 (solvent) at point A, and again $\theta_2 = \theta_1 + \frac{\pi i}{3}$. The mole fraction of the third component of any point can be found by applying our boundary equation, (2.6). The free energy of a homogeneous mixture at a given composition, say point C, is then given by (2.68), and the free energy of a phase separated mixture, $F(a, b, \theta_1)$, with our tie line through point C with endpoints A and B, is given by the lever rule:

$$F(a,b,\theta_1) = \left(\frac{a}{a+b}\right) G(A) + \left(\frac{b}{a+b}\right) G(B) \tag{2.76}$$

where the mole fractions at A and B are both dependent on point C and the angle θ_1, as well as b and a, respectively. Now we can calculate the change in the free energy of the "phased" system as we change one of the three tie line variables:

$$\begin{aligned}\frac{\partial F}{\partial a} &= \left[\frac{b}{(a+b)^2}\right][G(A) - G(B)] + \left[\frac{b}{a+b}\right] \times \\ &\quad \left[-\sin\theta_1 \left(\frac{\partial G}{\partial \phi_1}\right)_B + \sin\theta_2 \left(\frac{\partial G}{\partial \phi_2}\right)_B\right]\end{aligned} \tag{2.77}$$

$$\begin{aligned}\frac{\partial F}{\partial b} &= \left[\frac{a}{(a+b)^2}\right][-G(A) + G(B)] + \left[\frac{a}{a+b}\right] \times \\ &\quad \left[\sin\theta_1 \left(\frac{\partial G}{\partial \phi_1}\right)_A - \sin\theta_2 \left(\frac{\partial G}{\partial \phi_2}\right)_A\right]\end{aligned} \tag{2.78}$$

$$\begin{aligned}\frac{\partial F}{\partial \theta_1} &= \left[\frac{ab}{a+b}\right]\left\{\cos\theta_1 \left[\left(\frac{\partial G}{\partial \phi_1}\right)_A - \left(\frac{\partial G}{\partial \phi_1}\right)_B\right] - \right. \\ &\quad \left. \cos\theta_2 \left[\left(\frac{\partial G}{\partial \phi_2}\right)_A - \left(\frac{\partial G}{\partial \phi_2}\right)_B\right]\right\}\end{aligned} \tag{2.79}$$

where $\left(\frac{\partial G}{\partial \phi_1}\right)_B$ is the partial derivative of the homogeneous free energy with respect to ϕ_1, evaluated at point B.

By using (2.77)-(2.79), we can now find the most stable tie line through point C by minimizing the free energy of the tie line through that point. After minimization, we will find one of two possible outcomes for the tie line. If the tie line shrinks to a point, corresponding to $a = b = 0$, then we have found a homogeneous point in our system at point C, and we need to find another starting point. On the other hand, if we find a non-zero length tie line, we can begin our search for the next tie line near our previous one, but at some small distance away. By moving a small distance from the previous tie line each time, we will eventually generate the two-phase region containing the initial point C. The only limitations to this method is that regions of more than two phases are not easily distinguished, as we use tie lines explicitly in our calculations, and small two-phase regions are fairly difficult to find unless you already know where they should appear.

2.5 Polyelectrolyte Solution Simulations and Analysis

As a starting point, we used a reference system consisting of a polyelectrolyte chain consisting of 1000 segments, of which only one will become ionized in solution with a valence of +1. The added salt will be a symmetric binary salt of valence ± 1, such as NaCl. With the addition of a few additional parameters, we determined our parameter values for our initial simulation:

$$N = 1000, m = 1 \quad , \quad q = 1, \chi = 1.00$$

$$Z_\alpha = +1, Z_\beta = -1 \quad , \quad r_{\alpha s} = 0.5, r_{\beta s} = 0.5$$

$$\frac{e^2\beta}{2\varepsilon \mathrm{v}_1} = 0.119$$

where the last parameter given is based upon the solvent dielectric properties and the temperature. The result of this simulation can be seen in Figure 2.3, where each calculated tie line is shown. The shape of the curve is very reminiscent of a polymer-solvent-nonsolvent (P-S-NS) ternary phase diagram, with the salt as the "solvent" and the solvent as the "nonsolvent". This makes sense, as the high value chosen for χ means that our solvent is a poor solvent, while the effective binary interaction parameter between the salt ions and the polymer is very low, which only arises indirectly through the κ term. Also, the diagram is smooth as we go between tie lines, meaning that there are probably no regions of the phase diagram with three or more phases in equilibrium, which our program would probably show as a region of chaotic tie lines. Figure 2.3 will be the reference diagram for all comparisons between phase diagrams, at least for our initial results.

Now that we have a basis for comparison, let us look at the effect of the polymer parameters on the phase behavior. If we change the interactions between the polymer and the solvent, χ, we would expect the two-phase region to grow and shrink as we increase and decrease χ, respectively. As shown in Figure 2.4, we do, in fact, see this happening in our simulations, as expected. This is not surprising at all, since Flory-Huggins theory alone would predict this result. Similarly, if we change the length of the polymer, N, we would expect the two-phase region to grow and shrink as we make the chain longer and shorter, respectively. In our simulations, as we reduce the chain length, as shown in Figure 2.5, we recover this behavior. Again, simple Flory-Huggins theory would predict this behavior. We also tried to simulate chains of length 10, 15, and 20 segments, at different values of χ, and found similar results to those seen in Figures 2.4 and 2.5. The results from $N = 10$ are shown in Figure 2.6. However, while this is what we would expect from a simple mean field theory, the shortness of the chains make the location of

the charged segment very important, and the smearing of the charge over the whole chain becomes an unsupportable assumption. Therefore, all simulations of short chains are inherently suspect.

In addition to the nonionic parameters for the polymer, we also looked at the effect of the charge of the polymer by varying the number of sites that are charged, m, and varying the charge of the ionized site and counterion, q. For the number of sites, we generated the results shown in Figure 2.7. As we can see, it seems that increasing the charge of the chain makes the solution more miscible. When we change the charge of the sites and counterions, as opposed to the number of charged sites, and assuming only one ionized site ($m = 1$) per chain, we find no discernable change in the diagram from Figure 2.3. If we increase the number of ionized sites to $m = 10$, however, we find that high charges of the sites (such as $q = 4$) make the solution more immiscible, not more miscible, as shown in Figure 2.8. While the charge of the ionized sites cannot normally reach such high values, the theoretical results seem to contradict our finding of increased miscibility for increased charge on the polymer. It turns out that the reason for the discrepancy is because the important characteristic here is not the total charge on the chains, but the charges of the mobile counterions. When the number of charged sites on the chain were increased, as in Figure 2.7, we assumed that the charge of each site will not change, and therefore the counterions to the chain will still have the same charge. However, when we increased the charge of the sites, and therefore the counterions, the situation is somehow changed. A more detailed explanation for this will be discussed shortly.

Now that we have looked at the effect of the polymer on the phase behavior of our solutions, we will next turn our attention to the effect of the added salt. Our original parameters assumed a lightly charged, symmetric salt. If we instead use

a symmetric salt of valence $Z_\gamma = \pm 2$, such as $MgSO_4$, we find that our solution is more immiscible, as shown in Figure 2.9a. However, upon a more careful analysis of the new phase diagram, we find that the two-phase region has not simply grown proportionally larger, as we saw for increased χ in Figure 2.4, but has instead stretched up and to the right, toward the polymer/salt axis. While this seems to be a minor effect, it is a completely reproducible result. If we use an valence of ± 3, such as $AlPO_4$, we find a phase diagram, as shown in Figure 2.9b, which is unlike any previous diagram generated. Obviously, the mobile ions have a large effect on the phase diagram when they have a high valence. If we use an asymmetric salt instead of a symmetric one, we can look at the effect of the concentration of various charges on the phase diagrams. For example, for a salt of valence +1/-2, such as Na_2SO_4, or +1/-3, such as Na_3PO_4, we find diagrams which are virtually identical to our original salt, as shown in Figure 2.10a-b. This shows that even if an ion has a high valence, a large concentration of low-valence ions will overshadow the effect of the high-valence ions. This also helps to explain the effect of the charged chains, since a large molecule with many charged sites will be more miscible in our solutions if the sites (and counterions) have a low valence, and less miscible if those sites are highly charged. Also, similar to our ± 2 and ± 3 salts, we can use a salt of valence +2/-3, such as $Mg_3(PO_4)_2$ to find a diagram as shown in Figure 2.10c. As we might expect, the diagram falls somewhere between those of valence ± 2 and ± 3 and shows us that the diagram is still smooth over all ranges of mole fractions.

We have yet to explain how the new phase diagram comes about. To answer this question, we looked at the effect of χ on the +2/-3 salt diagram, as shown in Figure 2.11. As the polymer and solvent become more chemically compatible (i.e. lower χ), the single large two-phase region pinches together in the middle, creating two smaller two-phase regions. This effect is most evident in Figure 2.11c.

The region protruding from the polymer/solvent axis, at the bottom of the diagram, corresponds to our original P-S-NS diagram that we observed in our original solutions. The other two-phase region looks similar to the first region, with the exception that it is protruding from the polymer/salt axis. This shows that higher charges of the free ions from the salt causes our mixture to be more immiscible, especially for high concentrations of those ions. In fact, even if the polymer and solvent become miscible ($\chi \leq 0.5$), causing the lower two-phase region to disappear, the upper region will remain, as shown in Figure 2.11d. Conveniently, this theory is also a valid explanation of what was shown in Figure 2.8 for increasing charge of the counterions. As we increase the charge of the counterions, the system was more immiscible, especially when we increased the concentration of the counterions by increasing the number of ionizing sites on the polymer. In fact, this is probably the origin of the "salting-out effect" mentioned in the introduction.

2.6 Conclusions

This chapter examines the phase behavior of a polyelectrolyte solution in the presence of added salt. We assume that mean-field behavior will occur, allowing us to use the Flory-Huggins and Debye-Hückel theories to model the nonionic and ionic interactions, respectively. Ternary phase diagrams are calculated for a multitude of variations on our base system.

We have modeled the system of a polyelectrolyte in a solvent in the presence of salt as a ternary system, using Flory-Huggins theory to model the nonionic interactions and Debye-Hückel theory to model the electrostatic interactions of the salt ions, charged polymer chains, and counterions to those chains. For low charges in the system, we see a phase diagram similar to Flory's P-S-NS phase diagram, with

our salt acting like Flory's "solvent" and our solvent acting like Flory's "nonsolvent". If we change the size of the polymer chains or the interaction between the polymer and the solvent, we see effects identical to those of an uncharged system. However, changing the charges in the system can have a dramatic effect on the phase behavior. For the charges on the polymer, increasing the number of charged sites will make the system more stable, due to the increased number of counterions of charge 1. If we instead change the charge of the salt ions, we can find a new "salting out" phase diagram, where above a certain concentration of salt, the system is completely phase separated, again due to the increased charges of the free ions in the system. We have also varied our previous parameters for our new diagram to find out more information about the true nature of this new phase behavior. It turns out that this new diagram comes from a combination of two separate two-phase regions, one at the low solvent limit, and the other at the low salt limit. As we increase the interaction parameter for the two-region diagram, we see these two regions stretch towards one another, eventually joining and filling out to form a single two-phase region, which eventually touches the $\phi_2 = 0.0$ axis, as we have already seen.

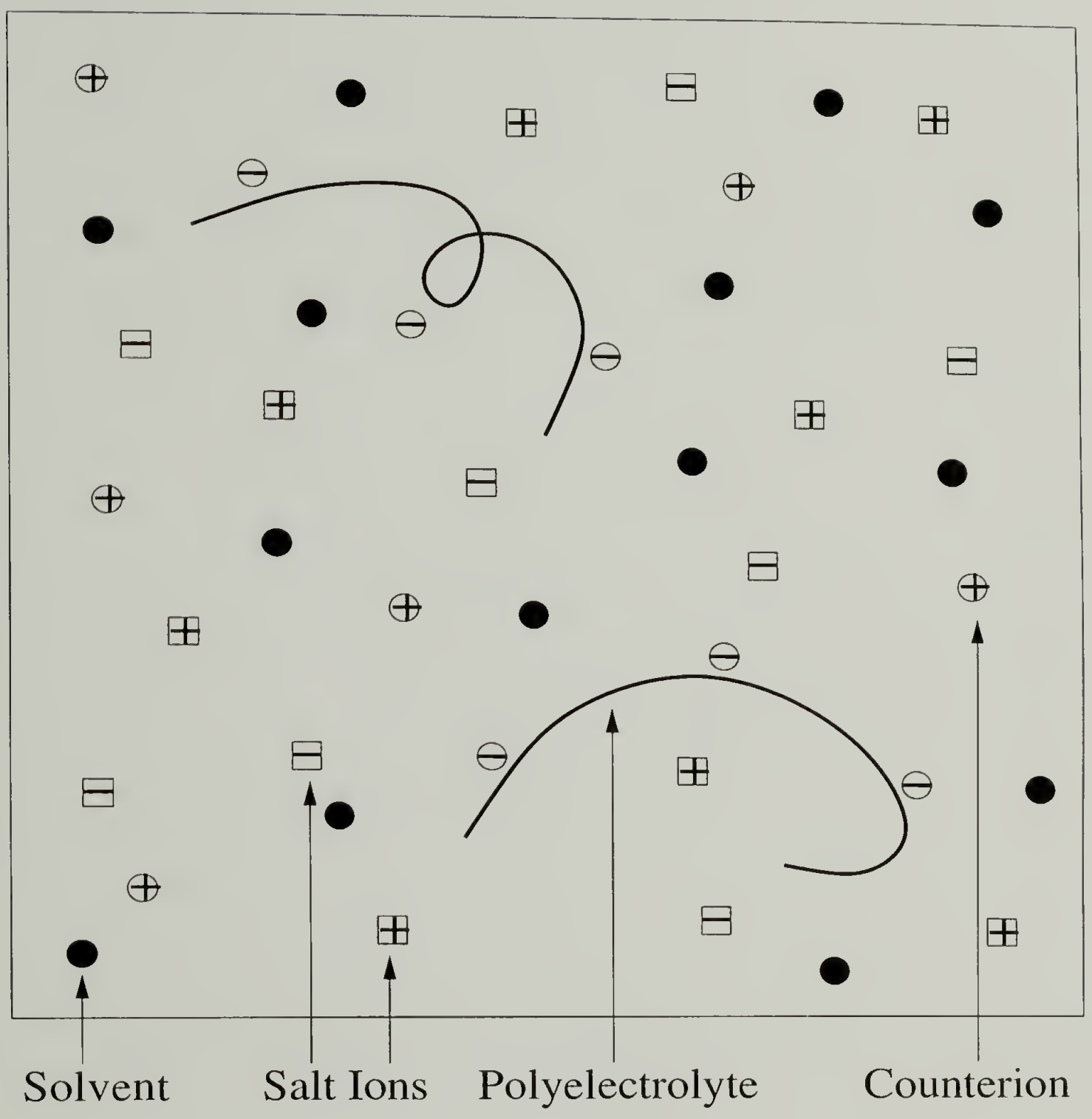

Figure 2.1. Pictorial representation of a polyelectrolyte solution. For the charges in the system, the squares represent the various salt ions, while the circles represent the charges on the polyelectrolyte chain and their corresponding counterions.

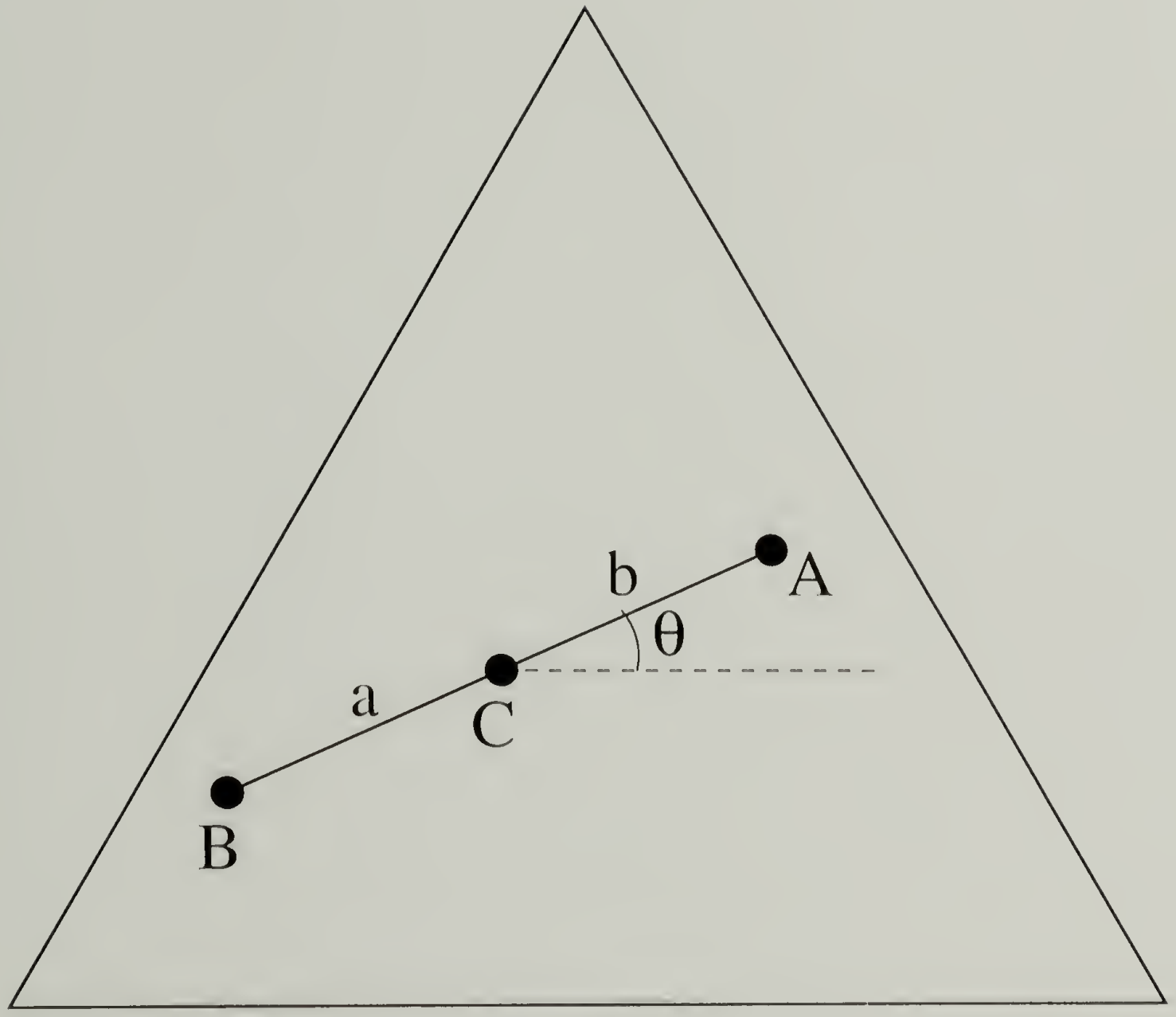

Figure 2.2. Graphical representation of a tie line, as defined in our compntational routines. Any tie line through a point C can be defined by the three parameters a, b, and θ.

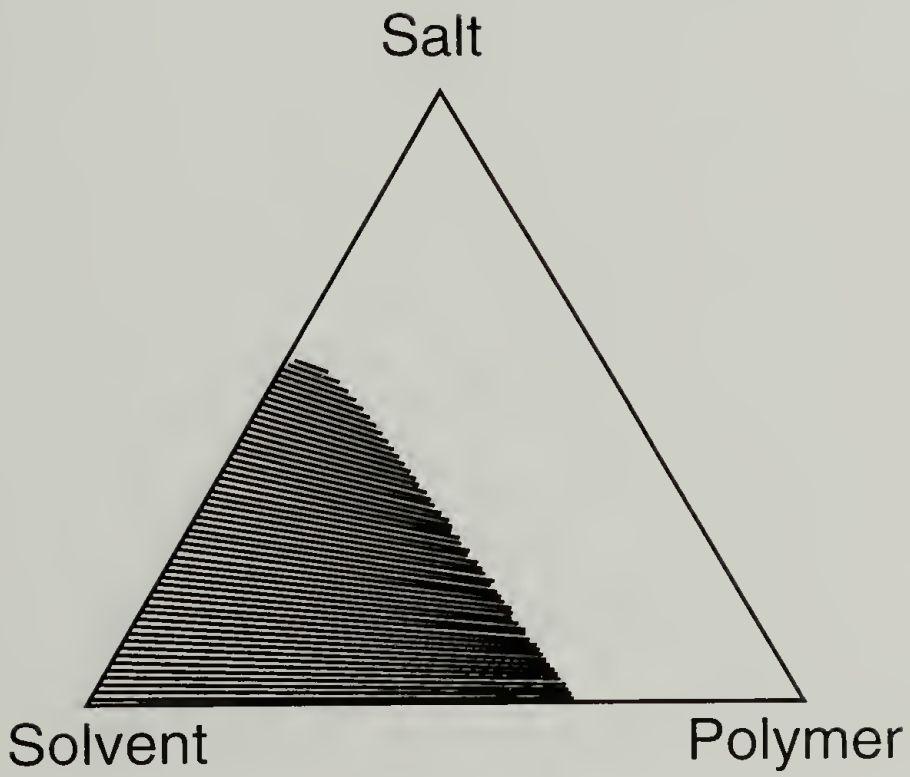

Figure 2.3. Phase diagram for $N = 1000$, $m = 1$, $q = 1$, $\chi = 1.0$, and a salt of the type X^+Y^-, such as NaCl. This diagram is taken as our reference point, and all axes are the same for all further phase diagrams presented.

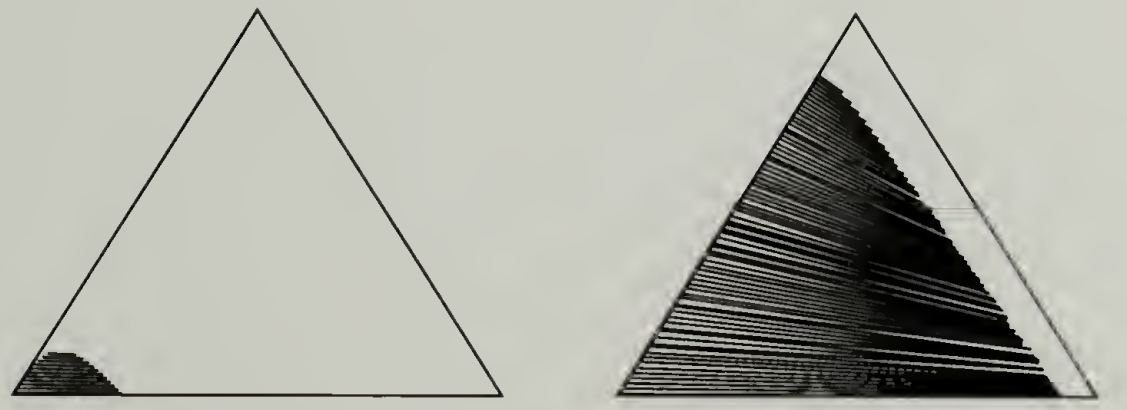

Figure 2.4. Phase diagrams for various polymer-solvent interaction parameters. (a) $\chi = 0.6$. (b) $\chi = 2.0$.

Figure 2.5. Phase diagrams for various polymer chain lengths. (a) $N = 200$. (b) $N = 50$.

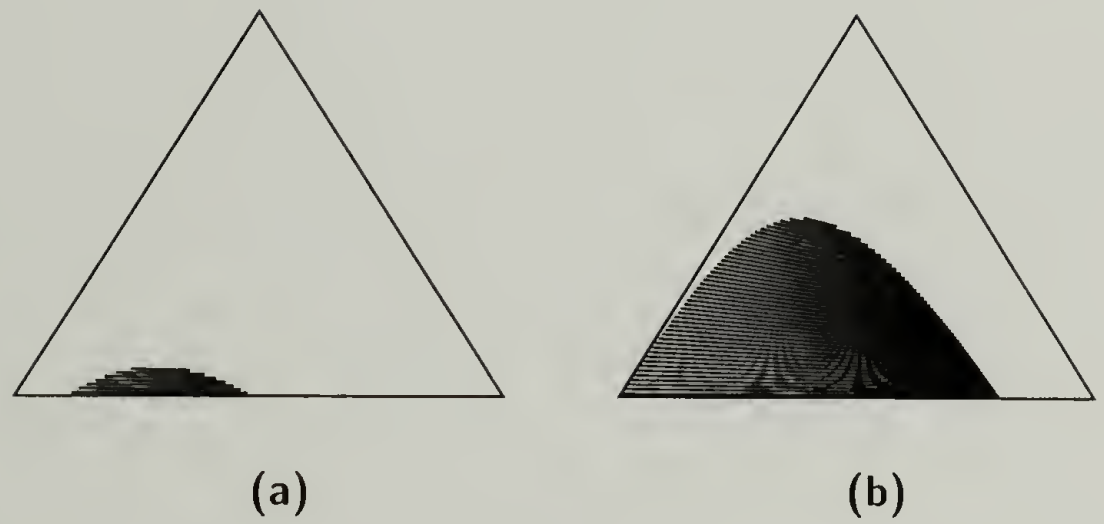

Figure 2.6. Phase diagrams for $N = 10$ and various polymer-solvent interaction parameters. (a) $\chi = 1.2$. (b) $\chi = 2.0$.

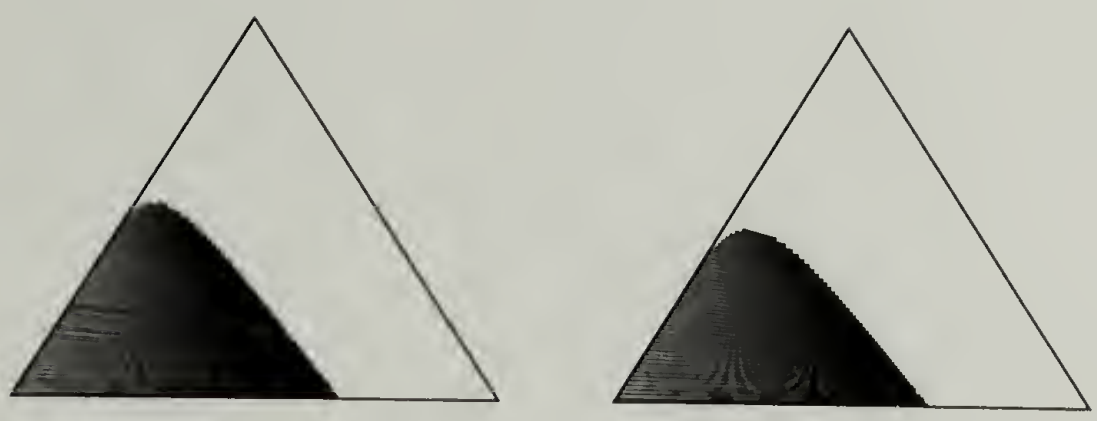

Figure 2.7. Phase diagrams for different numbers of ionized sites per chain. (a) $m = 5$. (b) $m = 10$. (c) $m = 20$. Note that the number of ionized sites per chain has no effect on the $\phi_s \rightarrow 0.0$ limit of the two-phase region.

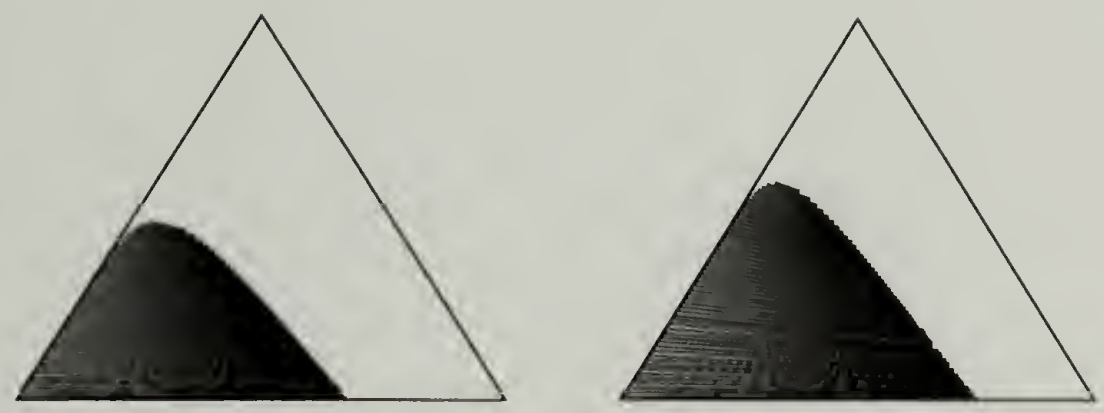

Figure 2.8. Phase diagams for $m = 10$ and different charges per ionized site. (a) $q = 2$. (b) $q = 4$.

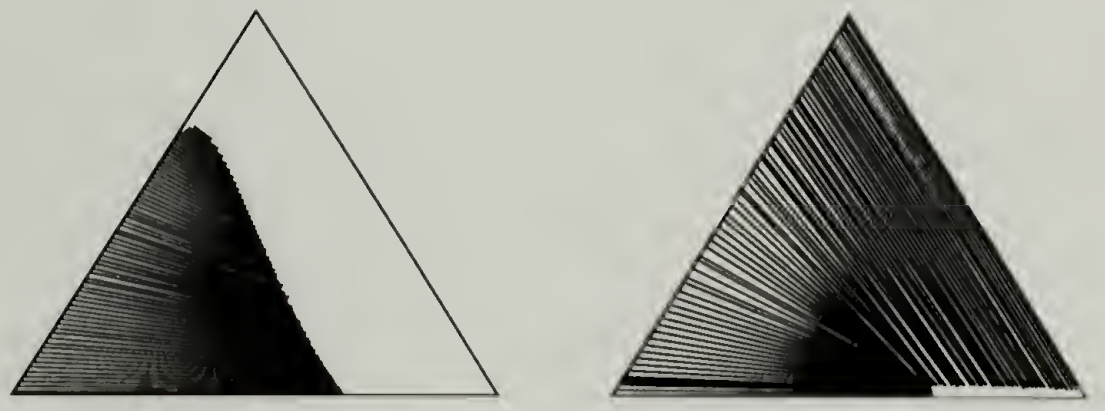

Figure 2.9. Phase diagrams for increased charge of salt ions. (a) $Z_\gamma = 2$, such as $MgSO_4$. (b) $Z_\gamma = 3$, such as $AlPO_4$.

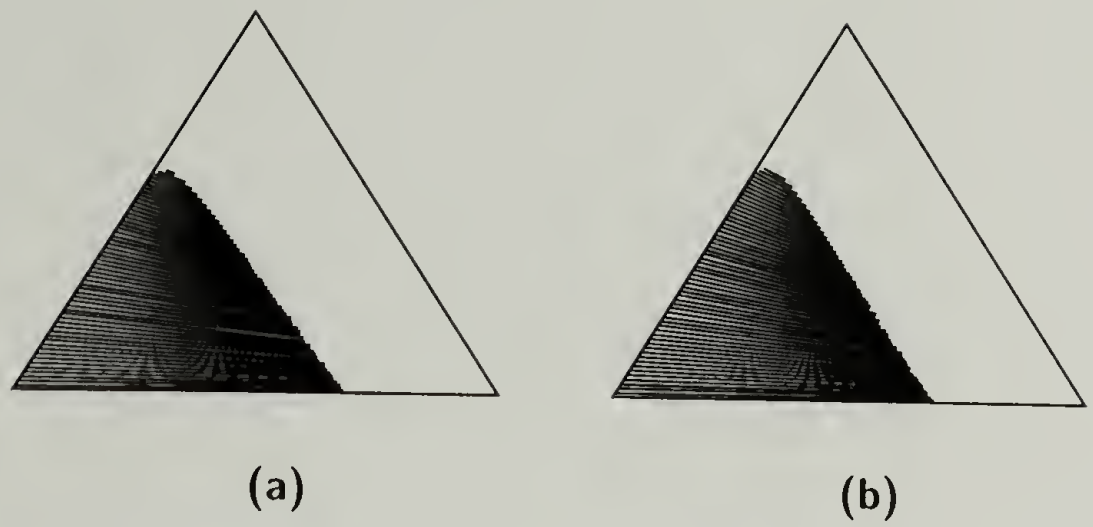

Figure 2.10. Phase diagrams for asymmetric salts. (a) $(X^+)_2Y^{2-}$, such as Na_2SO_4. (b) $(X^+)_3Y^{3-}$, such as Na_3PO_4. (c) $(X^{2+})_3(Y^{3-})_2$, such as $Mg_3(PO_4)_2$. Note that the diagram in (c) shows the "salting-out effect" described in the text.

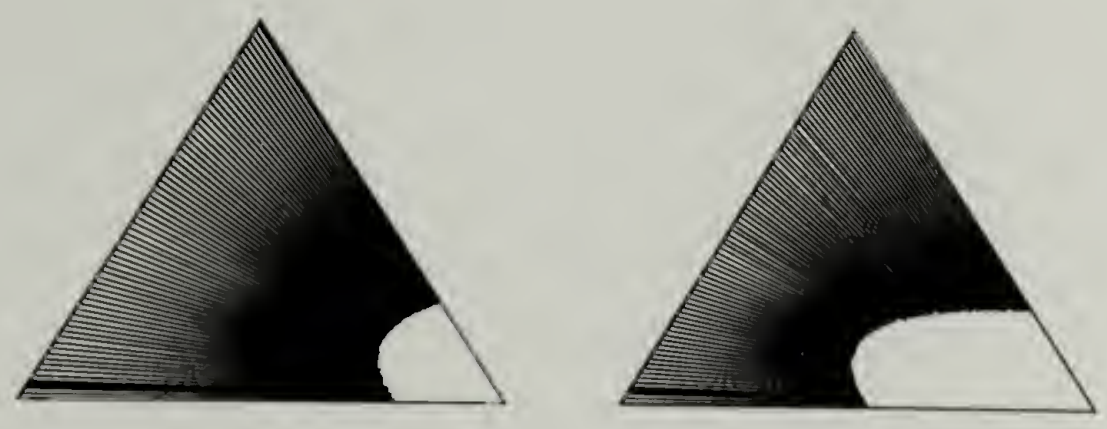

Figure 2.11. Phase diagrams for various values of χ for the new diagram (see Figure 2.10c). (a) $\chi = 1.2$. (b) $\chi = 0.8$. (c) $\chi = 0.6$. (d) $\chi = 0.3$.

CHAPTER 3

POLYELETROLYTE BRUSHES

3.1 Introduction

So far, we have been discussing solutions of free polyelectrolyte chains and salt in a solvent. This is only one area of interest, however. For example, colloid stabilization is another field of growing importance in which polyelectrolytes can be used. Specifically, by attaching the polyelectrolyte chains to a surface at a sufficient surface coverage, the chains will stretch out, and we obtain a polyelectrolyte brush on that surface. If two such surfaces are brought together, they will repel, both from steric interactions and from electrostatic interactions. Let us analyze what research has been done in this area.

Before we look at charged polymer brushes, we should first look at their neutral counterpart: uncharged brushes. Patel, Tirrell, and Hadziioannou [38] adsorbed a layer of poly(vinyl pyridine)-polystyrene block copolymer to a mica surface. In toluene, the poly(vinyl pyridine) block adsorbs to the surface and adopts a highly compact configuration, while the polystyrene block extends into the solvent. This allowed them to consider only the polystyrene block when determining the layer thickness. When they measured the force-distance profile for two such surfaces coming together, they found that as the two brush layers came together, there was a steric repulsion which depended on the size of the polystyrene block. Soon after

these experiments, Marra and Hair [39] performed similar experiments on adsorbed poly(ethylene oxide)-polystyrene block copolymers. For this block copolymer, the poly(ethylene oxide) adsorbed to the mica in the same manner as the poly(vinyl pyridine) had, but in this case, the toluene was a good solvent for the anchoring block, as well as the extending polystyrene block. The profiles, however, were very similar to those previously reported. However, in addition to toluene as the solvent, they also tried a toluene-heptane mixture as the solvent, where heptane is a poor solvent for both the poly(ethylene oxide) and the polystyrene blocks. They found that the quality of the solvent did indeed have a profound effect on the force profile between the adsorbed layers. In addition, they noted that for the mixed solvent, the compression and separation force profiles showed some hysteresis for the "better than θ solvent", which they attributed to the relaxation of polymer bridging between the surfaces.

In addition to the neutral brushes, there has also been some experimental work performed on polyelectrolyte brushes. For example, Lubetkin [50] performed experiments using poly(vinyl alcohol) adsorbed on mica surfaces in a concentrated aqueous salt solution ($1.0 \times 10^{-1} M$ KCl). As previously seen for neutral brushes, the force profiles for the polyelectrolyte brushes show a hysteresis, which yields repeatable results after the third separation of the surfaces. Unlike the previously mentioned experiments, these results were plotted on a semi-log plot, which shows that for the first compression, the force rises sharply at larger surface separation, then levels off somewhat to a gentle rise in the force for intermediate separations, and finally rises more sharply once again for short separations. For the third compression and separation, however, the final sharp rise in the force profile is no longer seen. A more detailed analysis, however, was performed by Luckham and Klein [47] for poly(L-lysine) adsorbed to a mica surface in a potassium nitrate (KNO_3) solu-

tion. The shape for the first compression and hysteresis for the following separation and for further compression/separation cycles were the same as for the poly(vinyl alcohol) brushes, for both a concentrated salt solution ($1.0 \times 10^{-1} M$) as well as for a less concentrated solution ($1.0 \times 10^{-3} M$). They further analyzed the shape of the curves to determine that the sharp rise in the force at larger distances corresponds to a profile of $F \sim \exp(-\kappa D)$, while the more gentle rise was a "slowing down" of the electrical double-layer overlap, while a steric compression of the adsorbed polyelectrolyte occurs. This latter effect was never quantified, however.

Although there has been much experimental work performed on polyelectrolyte brushes, most of the theoretical work that has been published has dealt with neutral polymer brushes. One of the most popular theories on this subject has been developed by Milner, Witten, and Cates [25]. By using a self-consistent field (SCF) method, they calculate the profile of a neutral brush attached to one surface in the "classical limit", corresponding to a strongly stretched brush at sufficiently high surface grafting of polymer chains. Since the chains should exhibit translational invariance parallel to the surface, they can model the brush in one dimension, perpendicular to the surface. They also assume the effective potential to be parabolic, which in turn leads to a parabolic brush profile. While this is an improvement over scaling theory approaches which use estimations of a step profile, this also was not sufficient in simulating a polymer brush. This is evident from an experiment performed by Kent, *et. al.* [17] in which they measured the density profile for Langmuir monolayers of polydimethylsiloxane-polystyrene block copolymers in ethyl benzoate. With the polydimethylsiloxane block adsorbing to the liquid-air interface, and the polystyrene block extending into the liquid phase, they used reflectivity to measure the density of the polystyrene blocks as a function of the distance from the surface. They found that both a depletion layer (lower density

near the surface) and an exponential tail (smoother density profile than parabolic when farther away from the surface) were evident from the results. In fact, some of the best results were seen using a skewed Gaussian curve to fit the data, as opposed to a parabolic curve, even when a depletion layer and exponential tail were added separately. However, the best results came from direct self-consistent field calculations. For example, Muthukumar and Ho [28] solved the Edwards path integral representation of the brush using a self-consistent algorithm. They were even able to incorporate excluded volume of the chains, both positive and negative, as well as an attractive or repulsive potential between the chains and the surface, thus giving a very accurate density profile for a brush on one wall under compression from either a bare wall or another brush-covered wall. These calculations were able to show both the depletion layer and the exponential tail as seen in the experiments.

Unfortunately, all of this work has been performed on neutral polymer brushes, not polyelectrolyte brushes. For the charged systems, Pincus [41] used a scaling approach to model polyelectrolyte brushes grafted onto two opposing surfaces. However, the force profiles arising from this method do not correspond to the measured profiles already described above. On the other hand, most theories [42, 45, 46] use a self-consistent field approach, and assume that the effective potential exhibits a parabolic profile, similar to the neutral brush case of Milner, Witten, and Cates [25]. Although this assumption has already been shown to be incorrect, the force profiles calculated by Miklavic and Marčelja [45] have a similar shape as that seen in the previously discussed experimental work. However, since direct self-consistent field calculations for polyelectrolytes have not been performed, similar to those of Muthukumar and Ho [28] for neutral brushes, these are the best results available to date.

In this chapter, we investigate the density and repulsive force profiles for poly-

electrolyte brushes. Specifically, we propose using a technique developed by von Goeler and Muthukumar [51] to model an unconstrained polyelectrolyte brush. If we assume Debye-Hückel interactions for the charges in the system, and that each chain will exhibit a similar density profile, then we can also assume that there will be uniform planes of charge due to the brush profile similarity. This allows the integration out of the directions parallel to the surface, leaving a one-dimensional analog to our brush, perpendicular to the surface. We can then perform a one-dimensional random walk to simulate the brush, allowing it to interact self-consistently in its own field, screened by the salt in the system. Instead of one surface covered with the brush, however, we can simulate two surfaces covered by the brush and constrained between the surface at a specific distance. By calculating the free energy of the confined brush as a function of the distance between the surfaces, we can then determine the force profile for a given salt solution. In addition, by following the density distributions, weighted by their statistical and energetic probabilities, we can also determine the density profiles of these brushes.

3.2 Continuous Chain Model for Polyelectrolyte Brushes

Before we begin explaining the theory of the polyelectrolyte brush in a salt solution, we must compare this model with that of a simple polyelectrolyte solution, as in our previous sections. As before, we have a number of charged polymer chains, with its corresponding counterions, immersed in a solvent with additional salt added. However, in this case one end of each chain will be attached to a solid surface, or "wall", which will not allow any penetration from a component of the system. In the case of an unconstrained brush, there is only one wall, and all segments of the polymer (aside from the one segment attached to the wall) will be on

one side of the wall, surrounded by solvent molecules, conterions, and various salt ions. For our system, we have two constrained brushes, with both walls having attached polymer chains extending into the area between the walls, again surrounded by the other chemical species. Since one of the units of each polymer chain has a fixed location, we cannot use a mean-field approach for the polymer units, as we cannot assume a random distribution of segments throughout our observed volume. Therefore, we will not use Flory-Huggins theory, as before. However, if we separate the mobile, or "free", chemical species from the "fixed" polymer, we will assume that the "free" molecules will be randomly distributed. While at first glance this seems to allow the use of Debye-Hückel theory, the charged polymer is not included, so we cannot use the theory as previously defined. However, if we group all of the mobile chemical species into a "background medium", then we can use Debye-Hückel theory to characterize a screening length for the background, κ, then let the charged polymer interact with itself through the medium. While we are changing our own theory a bit in doing this, it is still a reasonable asumption.

We will adapt a theory initially proposed by von Goeler and Muthukumar [51] to describe our system, composed of charged polymer chains grafted at one end to one of two parallel, planar, uncharged surfaces which are suspended in a salt solution. A picture of the system is given in Figure 3.1. Each chain is assumed to have an identical contour length, $L = Nl$, where N is the number of segments in each chain and l is the length of each segment. Also, each segment is assumed to carry an identical charge, q, and the charge is evenly distributed throughout the chain. Each surface has an identical uniform grafting density, σ, or number of chains per unit area, and the density is assumed to be large enough to cause a brush configuration for the polyelectrolyte, where the chains will be extended away from the wall. We finally define a Cartesian coordinate system by $z = 0$ at one of

the surfaces and $z = D$ at the other, with the z axis perpendicular to the surfaces; the x and y axes are parallel to the surfaces.

All segment-segment interactions are assumed to have two separate parts: the short-ranged excluded volume interactions, of strength $\bar{w}l$, and the long-ranged screened Coulombic interactions, of strength $\frac{\bar{v}}{l} = \frac{q^2 e^2 \beta}{\varepsilon}$, where again $\beta = \frac{1}{k_B T}$ and ε is the dielectric constant for the solvent, and range κ^{-1}, where κ is again the Debye screening length, as defined in (2.45) but using only the mobile (non-polymer) charges. We will represent the i^{th} polymer chain as a continuous curve, where the position of a given part of the chain is $\mathbf{R}_i(s)$ and s is the arc-length parameter for the chain along the chain's contour length, with $0 \leq s \leq L$. The connectivity of a given chain and the inter-segment interactions between units of that chain with units from both the same chain and other chains are now a function of the configurations of all of the chains in the system, $\{\mathbf{R}_i(s)\}$, and is given by the Edward's Hamiltonian:

$$\begin{aligned} H[\{\mathbf{R}_i(s)\}] &= \frac{3}{2l} \sum_i \int_0^L ds \left(\frac{\partial \mathbf{R}_i(s)}{\partial s} \right)^2 + \\ & \frac{1}{2} \sum_i \sum_j \int_0^L ds \int_0^L ds' V[\mathbf{R}_i(s) - \mathbf{R}_j(s')] \end{aligned} \tag{3.1}$$

where the first term represents the connectivity of the i^{th} chain and the second term represents the segment-segment interactions, with:

$$V[\mathbf{R}_i(s) - \mathbf{R}_j(s')] = \bar{w} l \delta[\mathbf{R}_i(s) - \mathbf{R}_j(s')] + \frac{\bar{v}}{l} \frac{\exp(-\kappa |\mathbf{R}_i(s) - \mathbf{R}_j(s')|)}{|\mathbf{R}_i(s) - \mathbf{R}_j(s')|} \tag{3.2}$$

where these terms represent the excluded volume and screened Coulombic interactions, respectively.

The probability of realizing a given configuration of chains is given by Boltzmann statistics:

$$P[\{\mathbf{R}_i(s)\}] = Z^{-1} \exp(-H[\{\mathbf{R}_i(s)\}]) \tag{3.3}$$

where Z is the partition function for this system:

$$Z = \int D[\mathbf{R}_i(s)] \exp(-H[\{\mathbf{R}_i(s)\}]). \tag{3.4}$$

Using Z, we find the free energy to be:

$$F = -\frac{1}{\beta} \ln Z \tag{3.5}$$

and therefore the repulsive force between the two surfaces, f, is given by:

$$f = -\frac{\partial F}{\partial D}. \tag{3.6}$$

Now we turn our attention to the configuration of a chain for our system. For a brush, one of the ends of the chain must be a grafting point, which we will denote as $\mathbf{R}_i(0)$, and will be attached to one of the two walls, either $z_i(0) = 0$ or $z_i(0) = D$. All other points on the chain must be located somewhere between the walls, or $0 < z_i(s) < D$ for $0 < s \leq L$. As each chain is a separate entity, we can see that (3.4) is a functional integral over the set of all chains in our system, which all conform to our boundary equations just described. Using the probability function given in (3.3), we can find the density profile of our brushes:

$$\langle \rho(\mathbf{r}) \rangle = Z^{-1} \sum_i \int D[\mathbf{R}_i(s)] \int_0^L ds \delta[\mathbf{R}_i(s) - \mathbf{r}] \exp(-H[\{\mathbf{R}_i(s)\}]) \tag{3.7}$$

where the sum is over all chains on both walls. For our calculations, it is possible to use a discretized version of (3.7) to calculate our density profiles for the polyelectrolyte, modelling the chains as a random walk in three dimensions. However, such a calculation would be excessively time-consuming. We note, however, that if all of the grafted chains are assumed to have the same or similar configurations, then only the density fluctuations perpendicular to the surfaces are of any real interest, since there are many other chains surrounding any given chain. Therefore, to

make our problem more tractable, we will assume that we have a uniform density distribution parallel to the surfaces. This is a reasonable assumption if we have a sufficiently high density of grafted chains, which we have already assumed to be true for any brush system. Using this assumption, we can look at a single pair of chains interacting with their own field, as opposed to all of the chains simultaneously, and assume planes of charge parallel to the surfaces, arising from the other chains in the system. Furthermore, we can now redefine our three-dimensional chains as one-dimensional continuous chains, which are allowed to fold back on themselves, perpendicular to the surfaces. Finally, all interactions between segments are also taken to be in one dimension. To convert our equations into their one-dimensional equivalents, we will integrate over the directions parallel to the surfaces. Thus, we can transform our Hamiltonian, (3.1), to:

$$\begin{aligned} H[\{z_i(s)\}] &= \frac{1}{2l}\sum_i \int_0^L ds \left(\frac{\partial z_i(s)}{\partial s}\right)^2 + \\ &\frac{1}{2}\sum_i \sum_j \int_0^L ds \int_0^L ds' V[z_i(s) - z_j(s')] \end{aligned} \tag{3.8}$$

where the segment-segment interactions are now:

$$V[z_i(s) - z_j(s')] = \frac{w}{l}\delta[z_i(s) - z_j(s')] + \frac{v}{\kappa l^3}\exp(-\kappa|z_i(s) - z_j(s')|) \tag{3.9}$$

with w and v both proportional to the grafting density and their original counterparts:

$$w = \sigma l^2 \bar{w} \tag{3.10}$$

$$v = 2\pi\sigma l^2 \bar{v}. \tag{3.11}$$

It should also be noted that the sums in (3.8) are now only for a single pair of chains, with one grafted on each surface, directly opposite each other. We can also

transform our density profile, (3.7), to one dimension as well:

$$\langle \rho(z) \rangle = Z^{-1} \sum_i \int D[z_i(s)] \int_0^L ds \delta[z_i(s) - z] \exp(-H[\{z_i(s)\}]) \tag{3.12}$$

where the one-dimensional partition function is now:

$$Z = \int D[\mathbf{R}_i(s)] \exp(-H[\{z_i(s)\}]) \tag{3.13}$$

with $\{z_i(s)\}$ being the pair of chains under observation. The equations for the free energy, (3.5), and the repulsive force, (3.6), are unchanged, except that they are now defined in only the z direction.

It should be noted that the assumption of a uniform distribution of chain segments, and therefore uniform planes of charge parallel to the surfaces, is only valid if the grafting density is sufficiently large. If the mean spacing between the grafting sites is more than the height of the brush, this assumption breaks down, as the chains are no longer in a "brush" configuration, but instead a "mushroom" configuration. If this happens, we can no longer assume a uniform plane of charge at a given distance from one of the surfaces, since there will be regions where there cannot be any chain segments. By assuming that we are working with a polyelectrolyte brush, however, avoids these concerns completely.

3.3 Random Walk Approximation and Computational Enumeration

Now that we have the one-dimensional continuous chain equations, , we need to convert them to equations for two discretized, one-dimensional random walks, one from each surface, to be used in our Monte-Carlo simulations. First, we will redefine

s and z in terms of the contour length and Gaussian chain size, respectively:

$$\frac{s}{Nl} \rightarrow s \tag{3.14}$$

$$\frac{z}{N^{\frac{1}{2}}l} \rightarrow z \tag{3.15}$$

and we will assume our segment length, l, to be 1, for convenience. This now lets us use s and z as dimensionless parameters which may only have integer values. Because each segment is connected to the previous one, the positions must be related by $z(s+1) = z(s) \pm 1$ since it must move exactly one unit in either the positive or negative z-direction with equal probability. We will define our boundary conditions to be that no segment may exist at the wall, $z(s) \neq 0$ and $z(s) \neq D$ with the exception of the grafted end, $s = 0$. Therefore, we can effectively ignore the grafted segment of each chain and simply let $1 \leq s \leq N$ and only allow positions of $1 \leq z \leq (D-1)$ for those segments. Because the grafted segment must be at either $z(0) = 0$ or $z(0) = D$ depending upon which wall the chain is grafted, the first recognized segment, $s = 1$ must be at $z(1) = 1$ or $z(1) = (D-1)$, respectively. In addition, since we know that we may not allow the following segment, $s = 2$, to go back into the wall, its location must be at $z(2) = 2$ or $z(2) = (D-2)$, respectively. Finally, for each subsequent segment thereafter, $3 \leq s \leq N$, if that segment is adjacent to the wall, $z(s) = 1$ or $z(s) = (D-1)$, the following segment must move away from the wall, $z(s+1) = 2$ or $z(s+1) = (D-2)$, respectively. Since the random walk would probabilistically hit the surface half of the time, we can speed up our calculations by forcing the correct step direction while the weighting factor for the chain, $\exp(-H[\{z_i\}])$, where $H[\{z_i\}]$ is again defined by (3.8), is multiplied by $\frac{1}{2}$. This is effectively the same as generating two equally probable chains, one of which hits the surface, and then throwing out that chain while keeping the chain with the allowed configuration, now of only "half strength".

Once a pair of chains have been built, one attached to each wall, we can find the density distribution for that specific pair by simply counting the total number of units at each allowed value of z:

$$\rho_m(z) = \sum_{i=\text{left}}^{\text{right}} \sum_{j=1}^{N} \delta_{z,z_{ij}} \tag{3.16}$$

where the i index corresponds to which surface a chain is attached, the j index corresponds to the s value along that chain, and $\delta_{z,z_{ij}}$ is the Dirac delta function. It should be noted the the subscript m corresponds to a specific configuration pair, as opposed to the average or overall values, as in (3.12). For a given configuration pair, we can find the Hamiltonian in terms of the assumed configurations. However, since we will be generating a large number of configuration pairs, we can also define the Hamiltonian for that pair to be that of a pair of chains in the presence of a potential field:

$$\begin{aligned} E_m[\{z_i(s)\}] &= \frac{1}{2} \sum_i \sum_j \sum_s \sum_{s'} V_m[z_i(s) - z_j(s')] \\ &= \frac{1}{2} \sum_z \sum_{z'} \rho_m(z) V_m(z - z') \rho_m(z') \end{aligned} \tag{3.17}$$

where we are now using our discrete model, and $V_m(z - z')$ is given by:

$$V_m(z - z') = w\delta_{z,z'} + \frac{v}{\kappa l} \exp(-\kappa |z - z'|). \tag{3.18}$$

and the connectivity, and therefore the entropy, of the chains are implicitly defined through the large sampling of random configurations. It should also be noted that the potential field arises from the distribution of chain segments, and therefore the distribution of charges, for the given configuration pair. For $z = z'$, we have to be very careful to avoid self interaction, or a given chain segment interacting, through either term in (3.18), with itself. In order to avoid this, we simply subtract 1 from the total number of segments for one of the segment densities at a given location

when $z = z'$, giving us:

$$E_m[\{z_i(s)\}] = \sum_{z<z'} \rho_m(z) V_m(z - z') \rho_m(z') + \frac{1}{2} \sum_z \rho_m(z) V_m(0) [\rho_m(z) - 1] \tag{3.19}$$

where the double counting in the first term has been avoided by requiring $z < z'$. The overall density distribution of chain segments may then be calculated by averaging over the ensemble of random walk pairs:

$$\langle \rho(z) \rangle = Z_E^{-1} \sum_{m=1}^{W} \rho_m(z) \exp(-E_m[\{z_i(s)\}]) \tag{3.20}$$

where the weighting factor is now in terms of the potential, E_m, instead of the Hamiltonian, H_m, and the new partition sum is now:

$$Z_E = \sum_m \exp(-E_m[\{z_i(s)\}]) \tag{3.21}$$

and both equations (3.20) and (3.21) have summations over the total number of generated random walk pairs, W. The reason we can use the potential instead of the Hamiltonian is that since the connectivity and interaction terms are additive in the Hamiltonian, they are separable, and become prefactors to the summations, and therefore cancel out in (3.20). This also conveniently avoids some of the approximations used in the mean-field theory. By using (3.21), we can calculate the free energy of a configuration pair, F, as well as the repulsive force between the surfaces, f, by (3.5) and (3.6), respectively. It should be noted that the free energy will not be the same for Z_E, in terms of the potential field only, as it would be for our original Z, in terms of the full Hamiltonian:

$$Z = Z_0 Z_E \tag{3.22}$$

where Z_0 arises from the connectivity of the pairs of chains and is assumed to be separable from the potential part, Z_E. However, the force will be the same, as it

only depends upon the change in free energy, which will have the connectivity as an added factor. If we perform the summation over a large number of configuration pairs, this sum will approximate an exact enumeration. We must be careful, however, to ensure that we generate enough configuration pairs to contain those near the free energy minimum; if the chains are normally highly stretched, we need to ensure that those stretched configuratione are generated in our simulations. As will be shown in the next section, however, this is not the case for our system.

3.4 Polyelectrolyte Brush Simulations and Analysis

In the course of our polyelectrolyte brush simulations, we modelled pairs of chains of various sizes, ranging from 16 to 128 segments. However, the best results from our simulations were mostly for chains of length 32 units, for determining density profiles, and 40 units, for determining force profiles. All results presented below will assume these values for their respective profiles. Also, for each simulation we built a total of $W = 10^6$ pairs of random walks to calculate our average density and force profiles. While it is possible that this number may not be sufficient for some systems, we will soon see that for our system, this number is sufficient.

Our computational routine was tested by calculating a neutral (Gaussian) chain, $v = 0$, of length $N = 400$ with varying strengths of the excluded volume interactions, w, and comparing the values with Muthukumar and Ho's published results [28]. The results show the routine to be accurate within reasonable expectations. For the purpose of our calculations, however, we assume that there is no excluded volume interactions ($w = 0$). This is a reasonable assumption, as the Coulombic forces at such short ranges will normally overshadow any excluded volume inter-

actions. In addition, we have set the strength of the Conlombic interactions to be $v = 2^{-6}$ in all of our simulations.

3.4.1 Density Profiles

First, we will analyze the density distribution, $\langle \rho(z) \rangle$, for our system. For the following discussion, we will assume our chain length to be $N = 32$. In our simulations, similar profiles have been found for other chain lengths, as well. A plot some of the density profiles for $N = 32$ can be seen in Figures 3.2 and 3.3.

At large surface separation, eg. $D = 32$, and short Debye screening lengths, eg. $\kappa = 2^{+2}$, the charges on the chain are highly screened. Therefore, we find a Gaussian-like density profile for each chain, as shown in Figure 3.2a for the higher values of κ. As we increase the Debye screening length, eg. $\kappa = 2^{-2}$, we find the chain exhibiting self-repulsion between its similarly charges units at short ranges, thus causing a more stretched out density profile, as can be seen for smaller values of κ in Figure 3.2a and larger values of κ in Figure 3.2b. This behavior has been well described by von Goeler and Muthukumar in their paper on single-surface polyelectrolyte brushes. However, if we continue to increase the screening length even more, eg. $\kappa = 2^{-6}$, each pair of polyelectrolyte chains begin to exhibit inter-chain repulsion, in addition to the intra-chain repulsion. In order to minimize the free energy of the chains, the chains adopt a "pancake" configuration; the "left" and "right" chains are both collapsed onto their respective surfaces. This can be seen for the smaller values of κ in Figure 3.2b. One possible explanation for this is that since the Debye screening length is on the order of the size of the surface displacement (or larger), the chains on each surface are not only interacting with charged units in its own chain, as in the intermediate case, but now interact with charged units from the other chain, as well. As one chain is now repelled by the

other chain, the two chains minimize this energy by keeping as far away from the other chain (and therefore, the other surface) as possible. This causes the chains to flatten themselves against their respective grafted surface, i.e. adopt the "pancake" configuration.

At small surface separation, eg. $D = 14$, the chains are now confined in an even smaller gap, such that at short screening lengths, eg. $\kappa = 2^{+2}$, the chain units are evenly distributed across almost the entire separation. This is also explained by the pairs of chains minimizing their free energy by extensive interpenetration such that a uniform density can be achieved, thus minimizing the system's free energy. When the screening length is increased, eg. $\kappa = 2^{-2}$, the "pancake transition" is once again seen, and the chains begin to separate from each other and collapse onto their respective surfaces. These effects can be seen in Figure 3.3. Further increases in the screening length simply sharpen the density profiles.

3.4.2 Force Profiles

We will now examine the effect of the surface separation, D, and the inverse Debye screening length, κ, on the repulsive force between the brush-filled surfaces. For these calculations, we will assume our chain length to be $N = 40$.

A plot of the repulsive force, f, as a function of the surface separation, D, is shown in Figure 3.4. It should be noted that due to finite size effects, data calculated below $D = 12$ is highly suspect. As these curves seem to show an exponential profile, we have combined the two graphs in a semi-log plot, Figure 3.5, confirming our observations. We can also see that the slope of each curve in Figure 3.5 is somehow dependent on its respective value of κ; thus:

$$f \sim \exp[-\alpha(\kappa)D] \tag{3.23}$$

which can also be defined as:

$$\frac{\partial(\ln f)}{\partial D} \sim \alpha(\kappa) \tag{3.24}$$

with α being some unknown function of κ. Now, using this equation, we can determine the κ dependence of the force profile. If we plot the calculated slope of each curve in Figure 3.5 against their corresponding value of κ, as shown in Figure 3.6a, we find a power law dependence on κ, shown in Figure 3.6b to be:

$$\alpha(\kappa) \sim \kappa^{\frac{1}{2}} \tag{3.25}$$

In our plots, data obtained for $N = 64$ was also used to confirm our findings. Therefore, substituting (3.25) into (3.23), we find:

$$f \sim \exp(-A\kappa^{\frac{1}{2}} D). \tag{3.26}$$

where A is some unknown constant of proportionality.

This result seems to be in direct disagreement with the Guoy-Chapman theory, which states that two charged walls in the presence of salt experience a repulsive force of:

$$f_{GC} \sim \exp(-\kappa D). \tag{3.27}$$

There are, however, two important points that distinguish these two theories. First, our system consists of long, charged chains attached to a neutral surface, as opposed to a flat, charged surface. For intermediate values of D and intermediate to large values of κ in our simulations (e.g. $\kappa = 2^{-3} - 2^{+2}$), the chains exhibit a Gaussian profile, so the polyelectrolyte brush system is not equivalent to the Guoy-Chapman system. Second, even for low values of κ where we observe a "pancake" configuration, we must also note that the two walls are held very close together in our analysis, with a maximum separation of only twice the chain length. Thus, if we assume intermediate values of D, which is the basis for (3.26), the Guoy-Chapman

limit of large D is not applicable. In addition, in Figure 3.5, larger values of κ ($\kappa = 2^{-1} - 2^{+2}$) do show a sharper slope for large values of D, which may well give results similar to the Guoy-Chapman theory. However, the results for large D in our systems were very noisy, so no analysis in this range was possible.

3.5 Conclusions

This chapter examines the force and monomer density profiles between two similarly charged polyelectrolyte brushes. The case of two parallel, planar brushes with high grafting density on a neutral surface is considered. Specifically, the effect of electrolyte solutions on the density profile and repulsive force between is examinined.

When the brush surface displacement is large, we find three possible monomer density profiles, depending upon the Debye screening length of the electrolyte solution. At short screening lengths, corresponding to a high salt concentration, the monomer-monomer interactions are neutralized and the density profiles are Gaussian-like. At intermediate screening lengths, the chains begin to stretch. In this intermediate screening length regime, the chain configurations are controlled primarily by chain-chain repulsions between chains grafted to the same surface. For long screening lengths (compared with the seperation distance, D) the chains collapse onto their respective grafting surfaces. In this long screening length regime, the effect of long-ranged repulsions between chains grafted on opposing walls is important. In this case, the chains' density distribution adopts a minimum free energy "pancake" profile.

When the brush surface displacement is small, we see only two different density profile regimes, depending upon the value of κ^{-1}. At short electrostatic screening

lengths, we see a highly interpenetrating density profile which is fairly uniform across the seperation distance. At large screening lengths, the chains collapse (as in the case of large seperation distances) onto their respective grafting surfaces.

In the case of only repulsive short-ranged excluded volume forces (i.e. no electrostatic forces), the "pancake transition", as described above, is absent. At low values of the excluded volume parameter, w, the brush density profiles are Gaussian-like. At large values of w, the brushes become stretched. As the value of w is increased, the brushes become more and more stretched and the density profile tends to become uniform accross the seperation distance.

Calculations of the repulsive force (a.k.a. stabilization force) between the two grafted polyelectrolyte brushes show an exponential dependence upon the seperation distance. Monte Carlo analysis shows that within an intermediate seperation distance regime, $f \sim \exp(-A\kappa^{\frac{1}{2}}D)$. In addition, the repusive force between the surfaces is linearly dependent on v ($\sim \frac{q^2}{\epsilon k_B T}$).

In the present model, we assume a constant value of κ throughout the entire volume between the opposing surfaces, neglecting local fluctuations in κ. This approximation is valid when the local charge density is not large. Thus, in the "pancake" regime, where the polyelctrolyte density is large near the surfaces, the actual density profile may vary somewhat from the results presented here due to variations in κ near the surfaces. Also, the use of a one-dimensional model assumes that density fluctuations in the directions parallel to the surfaces are negligible. This assumption is valid when the grafting density is large. While it has been pointed out that parallel density fluctuations do exist [35], we believe that they do not substantially affect our results.

While preliminary force measurements between polyelectrolyte brushes [47] - [50] are consistent with the above results, direct quantitative comparison with experi-

ment is difficult for several reasons. First, in most cases, the charge density on the polyelectrolyte chains is not known exactly. For example, as the density profiles change, the degree of ionization may change correspondingly. Furthermore, typical force measurement experiments calculate the planar brush force profile by using the results of a somewhat different geometery (e.g. crossed cylindrical). Additionally, the forces observed in experiment may result partially from nonequilibrium effects; the relaxation time for a compressed brush in the overlapped regime may be large compared with experimental time scales. Clearly, more work, both theoretical and experimental, is needed in these important areas.

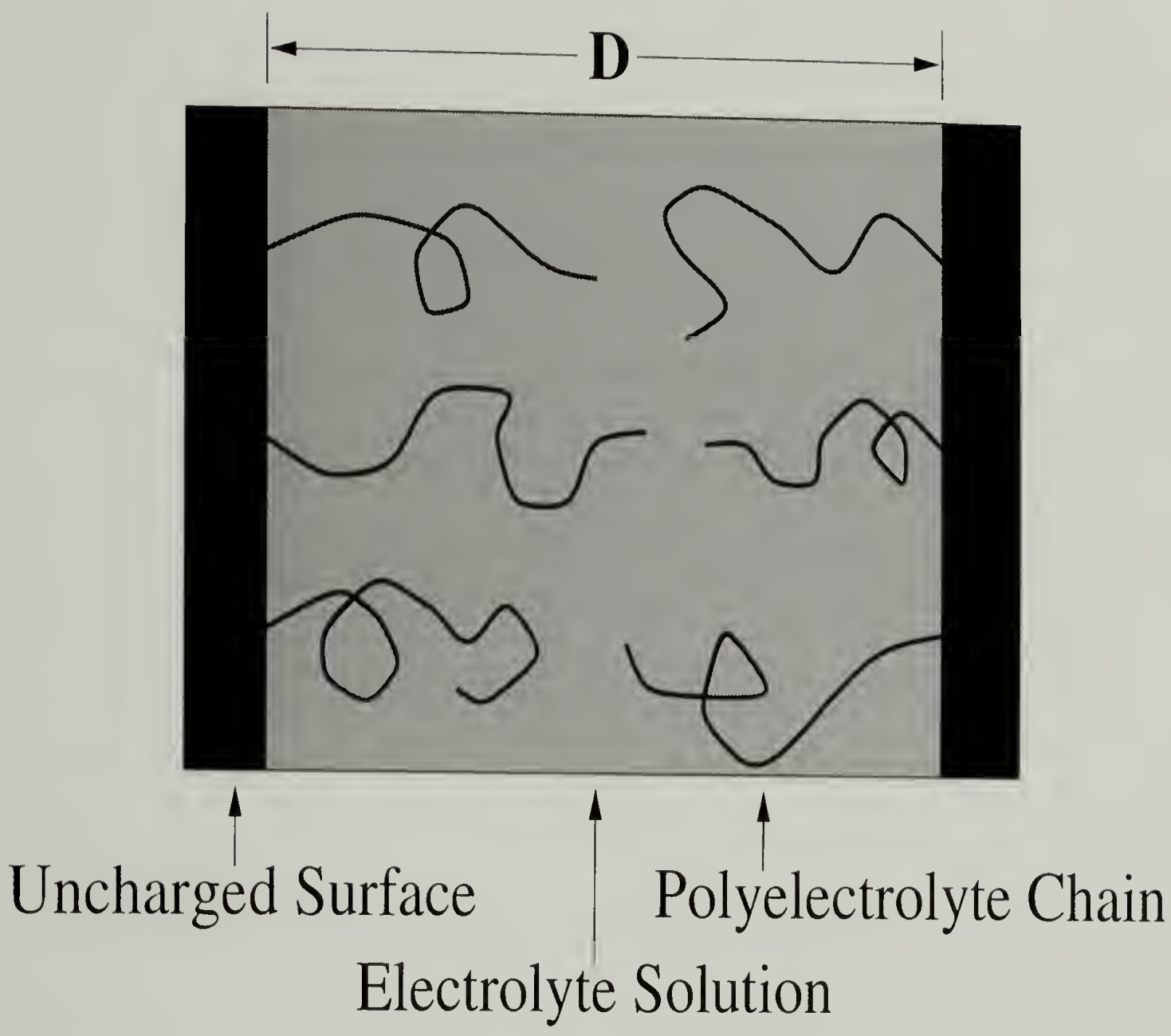

Figure 3.1. Pictorial representation of our polyelectrolyte brush system.

(a)

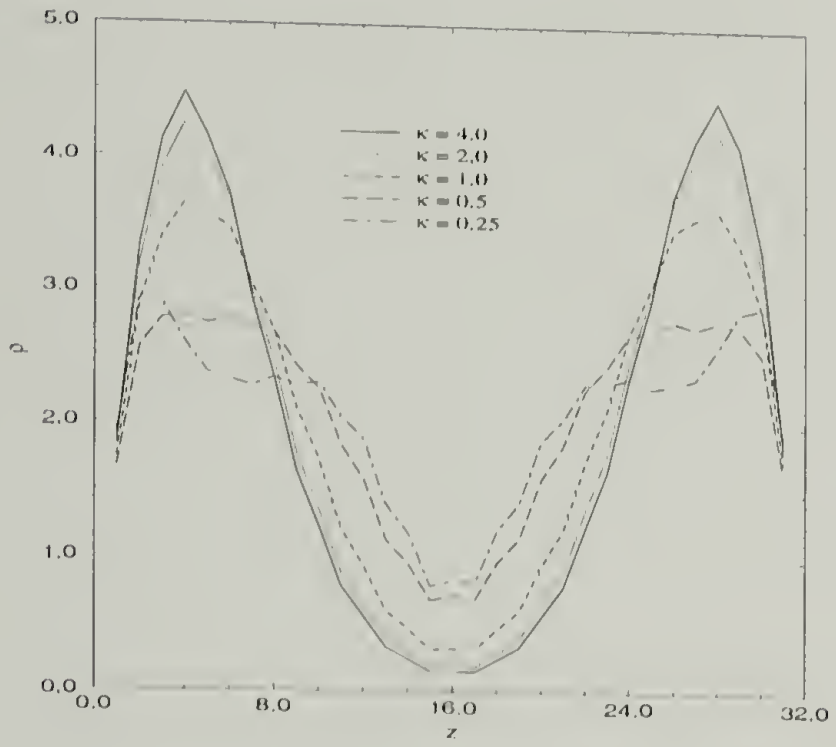

(b)

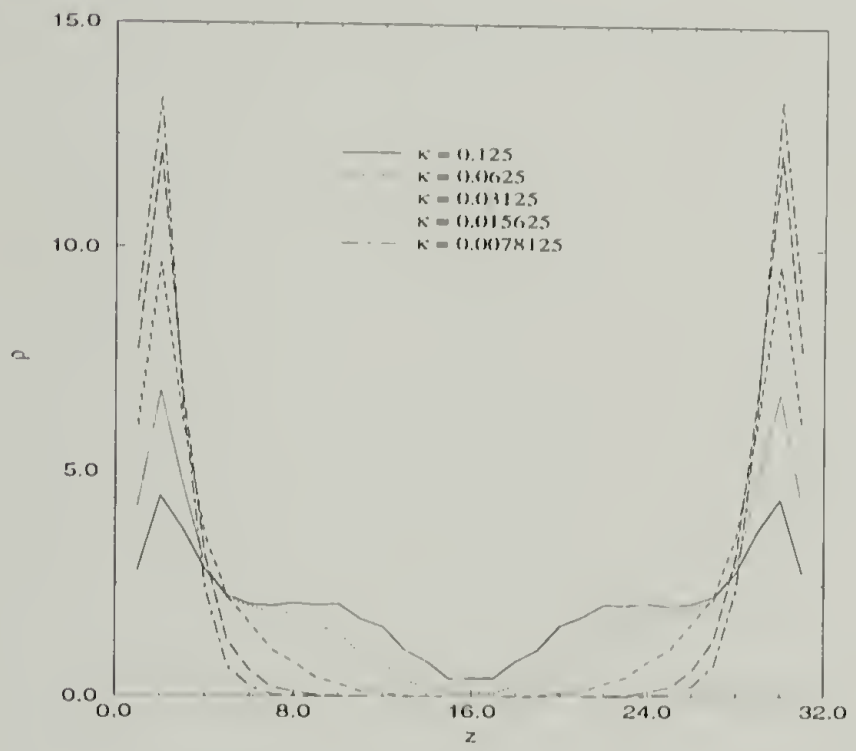

Figure 3.2. Density profiles for large surface separation. For both graphs, $N = 32$ and $D = 32$. (a) More concentrated electrolyte solutions [$\kappa = 2^{+2}$–2^{-2}]. (b) Less concentrated electrolyte solutions [$\kappa = 2^{-3}$–2^{-7}].

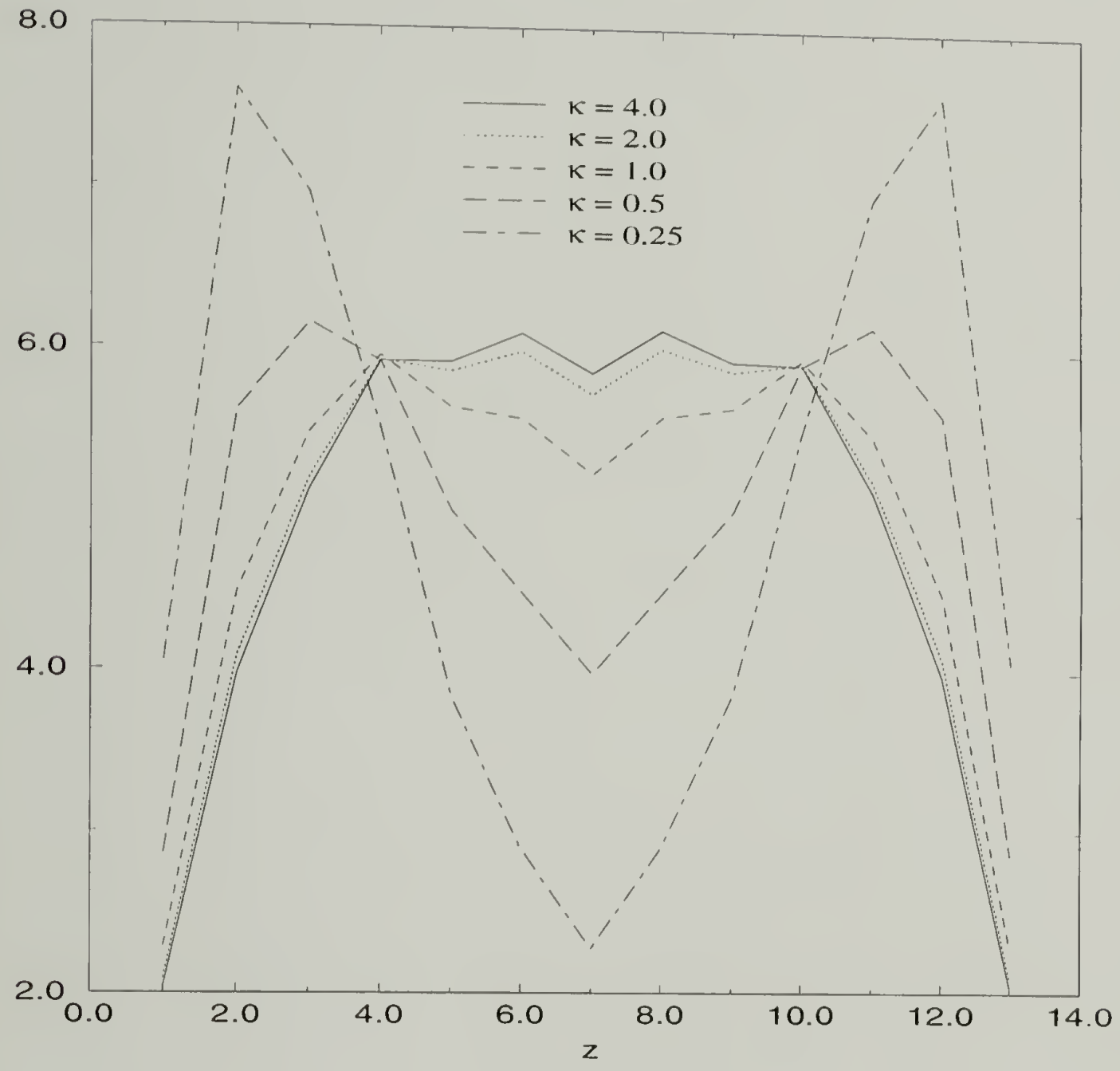

Figure 3.3. Density profiles for small surface separation, $D = 14$, and more concentrated electrolyte solutions, $\kappa = 2^{+2}$–2^{-2}.

(a)

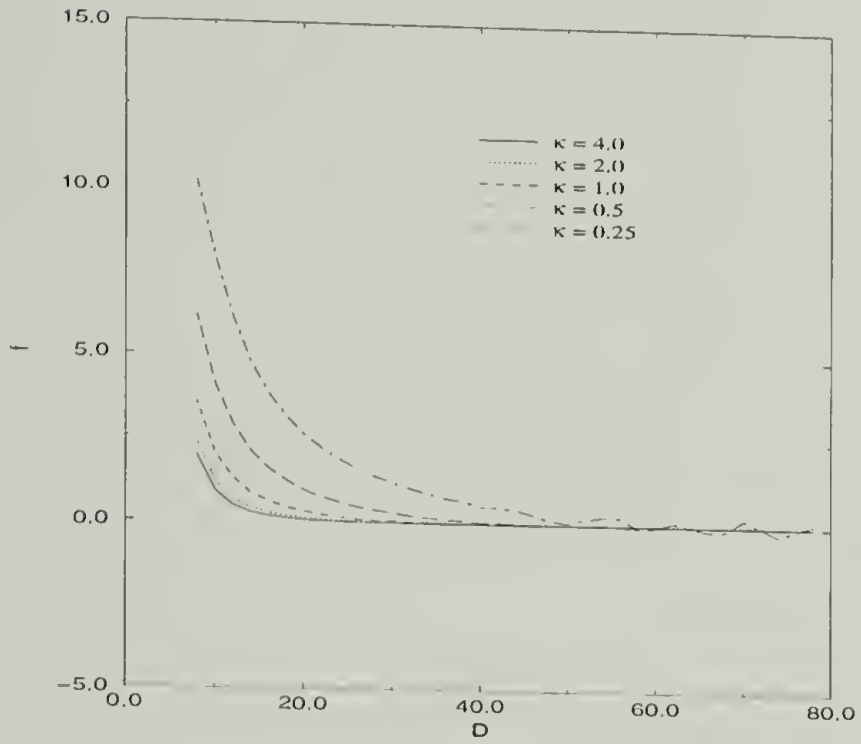

(b)

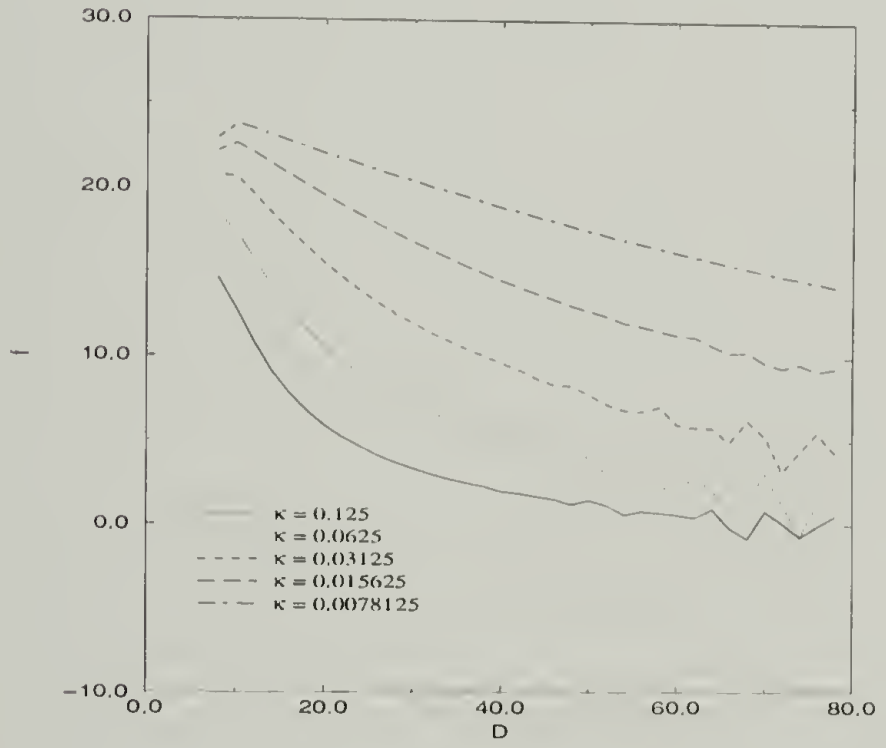

Figure 3.4. Repulsive force, as plotted against surface separation, for chains of length $N = 40$. (a) More concentrated electrolyte solutions [$\kappa = 2^{+2}$–2^{-2}]. (b) Less concentrated electrolyte solutions [$\kappa = 2^{-3}$–2^{-7}].

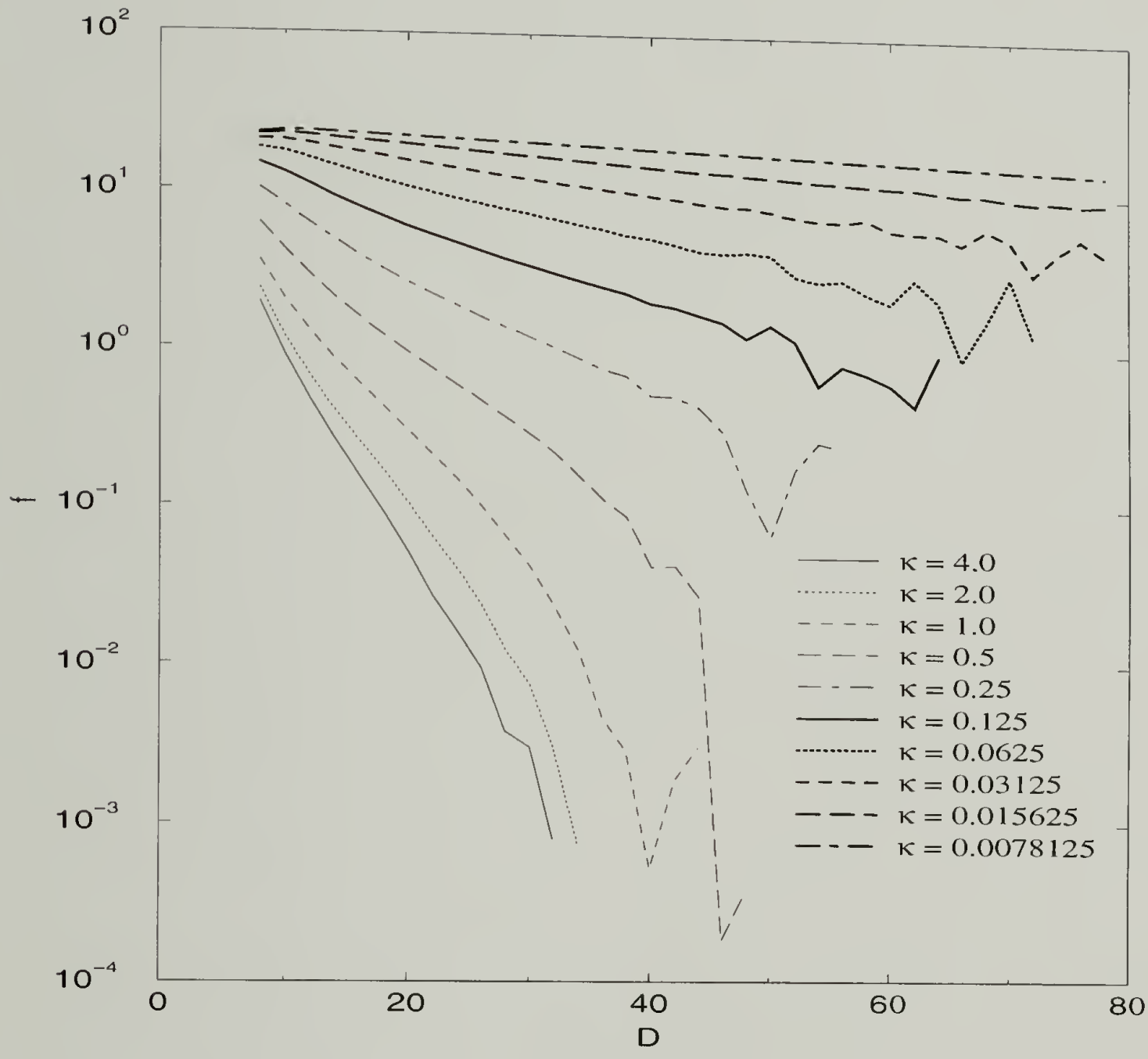

Figure 3.5. Semi-logarithmic plot of repulsive force vs. surface separation for $\kappa = 2^{+2}$–2^{-7}.

(a)

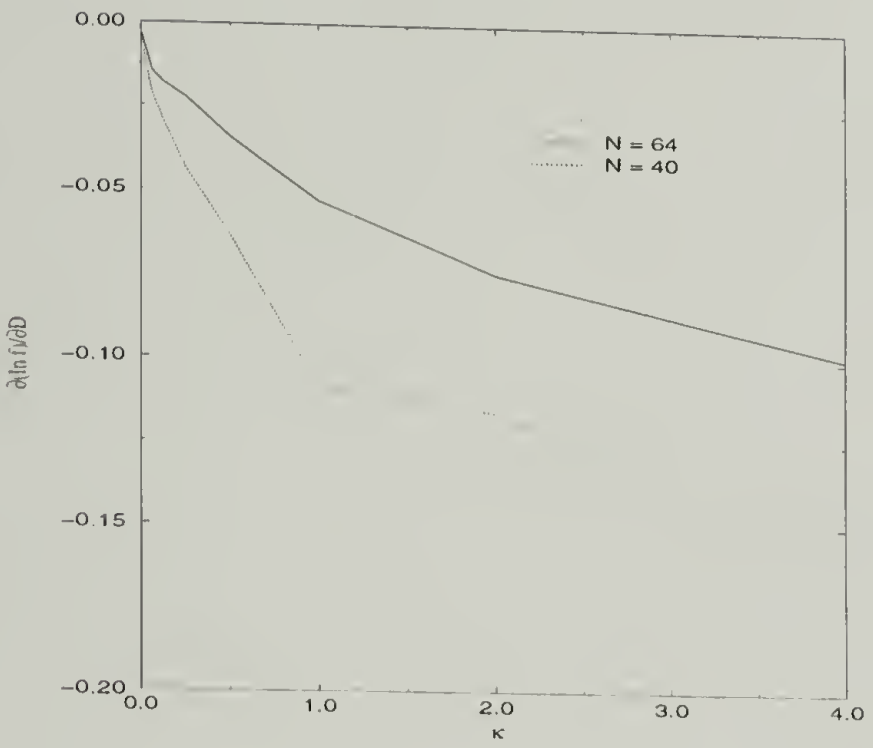

(b)

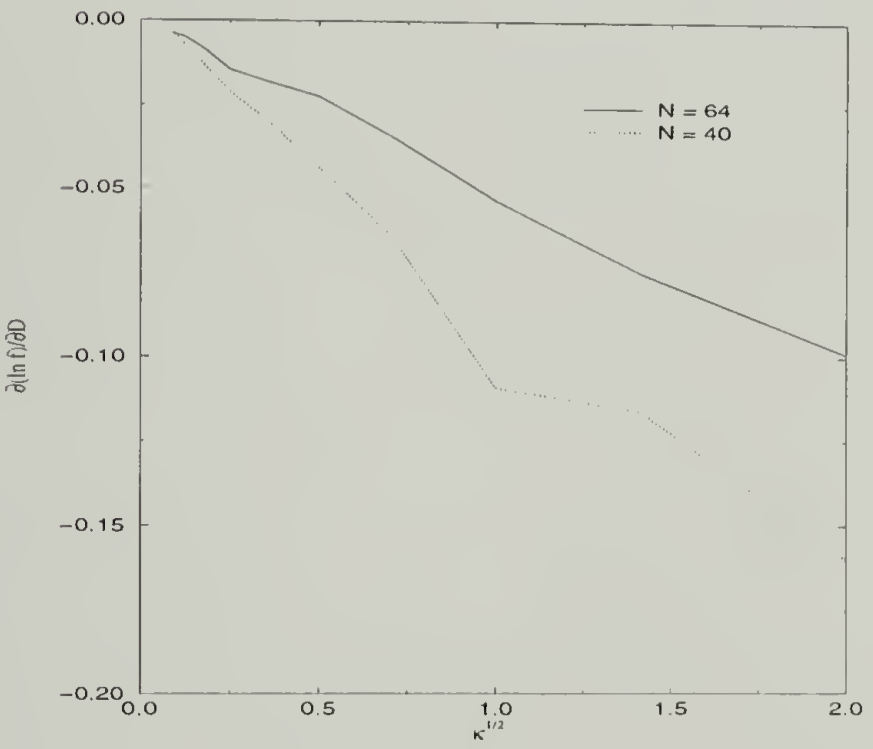

Figure 3.6. Plots of relation between $\frac{\partial(\ln f)}{\partial D}$ and κ. (a) $\frac{\partial(\ln f)}{\partial D}$ vs. κ. (b) $\frac{\partial(\ln f)}{\partial D}$ vs. $\kappa^{\frac{1}{2}}$.

BIBLIOGRAPHY

[1] S. C. Lin, W. I. Lee, and J. M. Schurr, *Biopolymers* **17**, 1041 (1978).

[2] K. Zero and B. R. Ware, *J. Chem. Phys.* **80**, 1610 (1984).

[3] M. Drifford and J.-P. Dalbiez, *Biopolymers* **24**, 1501 (1985).

[4] X. Li and W. F. Reed, *Biopolymers* **28**, 1981 (1989).

[5] X. Li and W. F. Reed, *Biopolymers* **30**, 1101 (1990).

[6] K. S. Schmitz, M. Lu, N. Singh, and D. J. Ramsay, *Biopolymers* **23**, 1637 (1984).

[7] M. Sedlák, *Macromolecules* **26**, 1158 (1993).

[8] M. Sedlák and E. J. Amis, *J. Chem. Phys.* **96**, 817 (1992).

[9] M. Sedlák and E. J. Amis, *J. Chem. Phys.* **96**, 826 (1992).

[10] N. Th. M. Klooster, F. van der Touw, and M. Mandel, *Macromolecules* **17**, 2070 (1984).

[11] P. J. Flory, *Principles of Polymer Chemistry*, Cornell University Press, Ithaca, pp. 495-511, 541-563 (1953).

[12] eg. see R. Koningsveld and L. A. Kleintjens, *Macromolecules* **4**, 637 (1971).

[13] P. M. V. Resbois, *Electrolyte Theory*, Harper & Row Publishers, New York, pp. 26-39 (1968).

[14] J. Skolnick and M. Fixman, *Macromolecules* **10**, 944 (1977).

[15] T. Odjik, *Polymer* **19**, 989 (1978).

[16] M. Muthukumar, *J. Chem. Phys.* **86**, 7230 (1987).

[17] M. S. Kent, L. T. Lee, B. J. Factor, F. Rondelez, and G. S. Smith, *J. Chem. Phys.* **103**, 2320 (1995).

[18] D. H. Napper, *Polymeric Stabilization of Colloidal Dispersions*, (Academic, New York, 1983).

[19] A. Halperin, M. Tirrell, T. P. Lodge, Adv. in Polymer Science, **100**, 1992 (1991).

[20] S. Milner, Science, **251**, 905 (1991).

[21] J. Isrealachvilli, *Intermolecular and Suface Forces with Applications to Colloidal and Biological Systems*, (Academic, London, 1985).

[22] A. K. Dolan, S. F. Edwards, Proc. R. Soc. London, A, **337**, 509 (1974).

[23] S. Alexander, J. Phys. (Paris), **38**, 983 (1977).

[24] P. G. de Gennes, Macromolecules, **13**, 1069 (1980).

[25] S. T. Milner, T. A. Witten, M. E. Cates, Macromolecules, **21**, 2610 (1988).

[26] E. Zhulina, O. Borisov, V. Priamitsyn, J. Colloid and Interface Sci., **137**, 495 (1990).

[27] C. M. Wijmans, J. M. H. M. Scheutjens, E. B. Zhulina, Macromolecules, **25**, 2657 (1992).

[28] M. Muthukumar, J. Ho, Macromolecules, **22**, 965, (1989).

[29] M. A. Carignano, I. Szleifer, J. Chem. Phys., **98**, 5006 (1993); M. A. Carignano, I. Szleifer, J. Chem. Phys., **100**, 3210 (1994); M. A. Carignano, I. Szleifer, Macromolecules, **27**, 702 (1994).

[30] T. Cosgrove, T. Heath, B. van Lent, F. Leermakers, J. M. H. M. Scheutjens, Macromolecules, **20**, 1692 (1987).

[31] G. Grest, M. Murat, Macromolecules, **26**, 3108 (1993); G. Grest, M. Murat, Macromolecules, **24**, 704 (1991); G. Grest, M. Murat, Macromolecules, **22**, 4054 (1989).

[32] A. Chakrabarti, R. Toral, Macromolecules , **23**, 2016 (1990); R. Toral, A. Chakrabarti, R. Dickman, Phys. Rev. E, **50**, 343, (1994).

[33] P. Auroy, L. Auvray, L. Leger, Physica A, **172**, 269 (1991); P. Auroy, Y. Mir, L. Auvray, Phys. Rev. Lett., **69**, 93 (1992).

[34] G. Hadziioannou, S. Patel, S. Granick, M. Tirrell, J. Am. Chem. Soc., **108**, 2869 (1986).

[35] G. Hadziioannou, private communications

[36] J. B. Field, C. Toprakcioglu, R. C. Ball, H. B. Stanley, L. Dai, W. Barford, J. Penfold, G. Smith, W. Hamilton, Macromolecules, **25** , 434 (1992).

[37] J. H. Taunton, C. Toprakcioglu, L. J. Fetters, J. Klein, Macromolecules, **23**, 571 (1990).

[38] S. Patel, M. Tirell, G. Hadziioannou, Coll. and Surf., **31**, 157, (1988).

[39] J. Marra, M. L. Hair, Coll. and Surf., **34**, 215, (1988).

[40] H. Watanabe, M. Tirell, Macromolecules, **26**, 6455, (1993).

[41] P. Pincus, Macromolecules, **24**, 2912 (1991).

[42] E. B. Zhulina, O. V. Borisov, T. M. Birshtein, J. Phys. II, **2**, 63 (1992).

[43] R. Isreals, F. A. M. Leermakers, G. J. Fleer, E. B. Zhulina, Macromolecules, **27**, 3249 (1994).

[44] O. V. Borisov, E. B. Zhulina, T. M. Birshtein, Macromolecules, **27**, 4795 (1994).

[45] S. J. Miklavic, S. Marcelja, J. Phys. Chem., **92**, 6718 (1988).

[46] S. Misra, S. Varanasi, P. P. Varanasi, Macromolecules, **22**, 4173 (1989).

[47] P. Luckham, J. Klein, J. Chem. Soc. Faraday Trans., bf 80, 865 (1984).

[48] H. Watanabe, S. S. Patel, J. F. Argillier, E. E. Parsonage, J. Mays, N. Dan-Braudon, M. Tirrell, Mat. Res. Soc. Proc., **249**, 255 (1992).

[49] M. Dahlgren, Langmuir, **10**, 1580 (1994); M. Dahlgren, A. Waltermo, E. Blomberg, P. Claesson, L. Sjostrom, T. Akesson. B. Jonsson, J. Phys. Chem. **97**, 11769 (1993); M. Dahlgren, P. Claesson, Nordic Pulp and Paper Research Journal, **1**, 62, (1993).

[50] S. Lubetkin, Coll. and Surf., **31**, 203, (1988).

[51] F. von Goeler, M. Muthukumar, Macromolecules, **28**, 6608 (1995); F. von Goeler, M. Muthukumar, submitted to J. Chem. Phys. (1995).

[52] M. Doi, and S. F. Edwards, *The Theory of Polymer Dynamics* , (Clarendon, Oxford, 1986).